EARTHQUAKE AND CONFLICT-RELATED URBAN DAMAGE ASSESSMENT USING COHERENCE CHANGE DETECTION WITH SENTINEL-1 IMAGERY

METHICHAI OBOM

A THESIS SUBMITTED IN PARTIAL FULFILLMENT OF
THE REQUIREMENTS FOR MASTER DEGREE OF SCIENCE
IN GEOINFORMATICS
FACULTY OF GEOINFORMATICS
BURAPHA UNIVERSITY
2024

การประเมินความเสียหายของเมืองจากแผ่นดินไหวและการสู้รบด้วยการตรวจจับการเปลี่ยนแปลงค่าโคฮีเรนซ์ร่วมกับภาพถ่ายดาวเทียมเซนทิเนล-1

เมธิชัย โอบอ้อม

วิทยานิพนธ์นี้เป็นส่วนหนึ่งของการศึกษาตามหลักสูตรวิทยาศาสตรมหาบัณฑิต
สาขาวิชาภูมิสารสนเทศศาสตร์
คณะภูมิสารสนเทศศาสตร์ มหาวิทยาลัยบูรพา
2567

EARTHQUAKE AND CONFLICT-RELATED URBAN DAMAGE ASSESSMENT USING COHERENCE CHANGE DETECTION WITH SENTINEL-1 IMAGERY

METHICHAI OBOM

A THESIS SUBMITTED IN PARTIAL FULFILLMENT OF
THE REQUIREMENTS FOR MASTER DEGREE OF SCIENCE
IN GEOINFORMATICS
FACULTY OF GEOINFORMATICS
BURAPHA UNIVERSITY
2024

The Thesis of Methichai Obom has been approved by the examining committee to be partial fulfillment of the requirements for the Master Degree of Science in Geoinformatics of Burapha University

Advisory Committee

Principal advisor

.....

(Professor Dr. Timo Balz)

Co-advisor

.....

(Dr. Kitsanai Charoenjit)

Examining Committee

.....

Principal examiner

(Professor Dr. Wolfgang Kainz)

.....

Member

(Professor Dr. Timo Balz)

.....

Member

(Dr. Kitsanai Charoenjit)

.....

Member

(Associate Professor Dr. Hong Shu)

.....

Acting Dean of the Faculty of Geoinformatics

(Associate Professor Dr. Arnon Wongkaew)

.....

This Thesis has been approved by Graduate School Burapha University to be partial fulfillment of the requirements for the Master Degree of Science in Geoinformatics of Burapha University

.....

Dean of Graduate School

(Associate Professor Dr. Witawat Jangiam)

.....

64910088: MAJOR: GEOINFORMATICS; M.Sc. (GEOINFORMATICS)

KEYWORDS: COHERENCE CHANGE DETECTION, URBAN DAMAGE ASSESSMENT, EARTHQUAKE, RUSSIA–UKRAINE CONFLICT

METHICHAI OBOM : EARTHQUAKE AND CONFLICT-RELATED URBAN DAMAGE ASSESSMENT USING COHERENCE CHANGE DETECTION WITH SENTINEL-1 IMAGERY. ADVISORY COMMITTEE: TIMO BALZ, KITSANAI CHAROENJIT 2024.

Disasters cause serious economic and human losses. Therefore, damage assessment is needed to support post-disaster management, humanitarian assistance, and disaster relief. This research focuses on applying the coherence change detection technique with Sentinel-1 data for damage assessment of urban areas of four cites. The first three cities affected by a natural disaster including Antakya, Iskenderun, and Adana in Turkey which affected form the two earthquakes of magnitude 7.8 and 7.5 occurred nine hours apart in south-eastern Turkey near the Turkey-Syria border on 6 February 2023. Another city affected by a human-caused disaster which is Mariupol, a city in the south-eastern Ukraine affected by the conflict between Russian and Ukraine since 24 February 2022 until the city was fully controlled by Russia in late May 2022.

For each study area, images of three months before the event were used. We used the images from November 2021 for Ukraine and November 2022 for Turkey. These images of three months until the last image before the event represent late autumn and winter seasons and were used to generate an average pre-event coherence image for each study area. Then, we applied a log ratio to the average pre-event and post event coherence image to find the intensity of coherence changes after the event occurred in each study area.

The results showed that the pre-event coherence of urban areas was high then turned to low after the earthquake, especially in Antakya, which was one of the most affected cities as the coherence decreased in all over the city, while Iskenderun showed loss of coherence mostly in the north-western part of the city as it was less affected than Antakya. The coherence of Adana slightly decreased as this city was least affected by the earthquake compared to the two cities. In Mariupol, there were

gradually changes in the beginning of the invasion, then a lot of changes occurred in middle March to middle May 2022 and the most intense changes happened in the city centre and the Azovstal industrial site. However, there also were widespread changes all over the urban areas.

The total area of Antakya affected by the earthquake was the most, at 44.58%. Iskenderun had the total affected area, at 24.09% and Adana had the least affected area at, 7.79%. In Mariupol, 44.88% of the urban area was affected by the conflict from the beginning of the invasion until June 2022. The coherence change detection technique with Sentinel-1 Imagery is a useful method in applying for damage assessment that can be used immediately during the early and critical state of disasters. It is suitable to identify changes in urban areas but not suitable to apply in areas that covered with vegetation.

ACKNOWLEDGEMENTS

I would like to acknowledge Ministry of Higher Education, Science, Research and Innovation for providing the SCGI Master Program scholarship.

I would like to express my sincere gratitude to my thesis supervisor, Professor Timo Balz, for your patience, guidance, and support as well as Dr Kitsanai Charoenjit, Dr Pattama Phodee, and Assistant Professor Dr Phattraporn Soytong, for their guidance throughout this thesis.

I would also like to thank Defence Information and Space Technology Department for granting permission for me to study this master's degree.

A special thanks to all my respected teachers and all members of the staff in Burapha University and Wuhan University for their kind support.

Many thanks to my parents and my friends for encouragement and support.

Methichai Obom

TABLE OF CONTENTS

Page

LIST OF TABLES

Page

LIST OF FIGURES

Page

CHAPTER 1
INTRODUCTION

Remote sensing data is useful for providing the latest information and helps in planning and management for important global issues such as climate change, disaster, and disease outbreak. This chapter includes a problem statement which aims to introduce the severity and impact of natural and human-caused disasters and how important remote sensing is in those emergency situations. This chapter also provides the overview of study areas as well as the objectives of this study. The final part of the introduction presents the overall structure of this thesis.

Statements and Significance of the Problems

In the period from 2000 to 2019, there were 7,348 major recorded disaster events claiming 1.23 million lives, affecting 4.2 billion people resulting in approximately US$2.97 trillion in global economic losses (United Office for Disaster Risk Reduction, 2020). On average, the majority of natural disasters each year are floods and storms, but the deadliest ones are earthquakes. The deadliest natural disasters of the past few decades were the Indian Ocean tsunami caused by an earthquake, which hit several countries in Asia in 2004, leaving 226,408 dead (United Nations, 2010). Human-caused disasters such as the massive explosion in Beirut, the capital and largest city of Lebanon, caused by a stockpile of ammonium nitrate stored in a port warehouse exploding on 4 August 2020, killing more than 200 people, wounding 7,000 people, destroying 77,000 apartments, displacing over 300,000 more, causing at least 80,000 homeless children, and also extremely severe (Office of the High Commissioner United Nations Human Rights, 2022b). Moreover, the conflicts in the world, from gang wars to ethnic violence, and from civil conflicts to world wars, lead the massive loss of lives, displacement of people, the disruption of economic system and the destruction of infrastructure and assets. After a catastrophic event, it is important to gather information as soon as possible to assess effects and impacts in order to provide emergency responses, recovery and reconstruction.

In the early hours of Monday 6 February 2023, Turkey faced two earthquakes of magnitude 7.8 and 7.5 which occurred nine hours apart in south-eastern Turkey near the Turkey-Syria border (Cappucci, 2023). These earthquakes resulted in widespread damage across 10 provinces of Turkey which designated by the Turkish authorities as disaster areas. The most heavily affected provinces are Hatay, Adiyaman and Kahramanmaras. The number of people who lost their lives in the earthquake is approximately 50,000 and the number of injured are more than 100,000 (United Nations Office for the Coordination of Humanitarian Affairs, 2023). This earthquake was extremely destructive and led to great loss in human life and suffering on an extreme scale.

On the night of 23 to 24 February 2022, the launch of the Russian military offensive made the security situation in Ukraine deteriorated rapidly (United Nations, 2022). The escalation of conflict had triggered an immediate and steep rise in humanitarian needs as essential supplies and services were disrupted and civilians fled the fighting. The UN estimated that 12 million people inside Ukraine would need relief and protection, while more than 4 million Ukrainian refugees might need protection and assistance in neighbouring countries in the coming months. The Government of Ukraine, the European Commission, and the World Bank, in cooperation with partners, estimated that the current cost of reconstruction and recovery in Ukraine amounts to US$349 billion. The Rapid Damage and Needs Assessment (RDNA) presented the first comprehensive evaluation of war impacts across twenty different sectors following the Russian invasion. It also presented the financing needs for a resilient, inclusive, and sustainable recovery and reconstruction and provided a roadmap for planning. The assessment covered the impacts of the war sustained between 24 February and 1 June 2022 and found that physical damage from the war reached over US$97 billion. It was particularly high in the housing, transport, commerce, and industry sectors (The World Bank, 2022).

Remote sensing can play an important role to support fast disaster response both natural and human-caused disasters. In the past few decades, thousands of Earth observation satellites have been launched into the space. There are two main types of remote sensing technologies including optical sensors and synthetic aperture radar (SAR) which can be applied to assess the damage after disasters. Optical sensors are

passive sensors which can deliver optical images that are easy to interpret visually. However, the optical sensors need sun illumination for imaging, and cannot penetrate clouds, which severely limits their application as an emergency tool. In contrast, SAR data are relatively difficult to interpret, and can be easily influenced by speckle noises. Nevertheless, they can be obtained both at night and in harsh weather conditions, owing to the active characteristics of SAR sensors and the long wavelength of the applied microwaves Therefore, SAR is considered to be more flexible and reliable for damage assessment at an early time following a disaster (Ge, Gokon, & Meguro, 2020). This spaceborne active sensor can be useful to let us see the damage of urban areas caused by any catastrophic events from the space view and help us analyse, manage, and respond to natural and human-caused disasters more efficiently.

This study focuses on applying SAR techniques to detect changes and destruction of urban areas caused by a natural disaster and a human-caused disaster which recently occurred in these few years. For a natural disaster, three cities affected form the Turkey earthquake in February 2023 are the study areas including Antakya and Iskenderun in Hatay province, the southernmost province of Turkey which is one of the most affected provinces by the earthquake and recorded ground motions associated with the earthquakes were very high. Another city is Adana in Adana province, located in the north of Hatay province which has less damage than Hatay province according to the report of the World Bank (Gunasekera et al., 2023). For a human-made disaster, the study area is the city of Mariupol in the south-eastern Ukraine. This city was affected by the conflict between Russian and Ukraine since Russia launched a military offensive in Ukraine on 24 February 2022, the city was attacked and under siege for over a month. The battle lasted until the city was fully controlled by Russia in late May 2022 (Psaropoulos, 2022). Sentinel-1 data and the coherence change detection (CCD) technique were used to process damage assessment in these study areas.

Objectives

1. To assess the damage of the urban areas of Antakya, Iskenderun and Adana affected by the earthquake using the CCD technique.

2. To assess the damage of the urban areas of Mariupol affected by the armed conflict between Russia and Ukraine using the CCD technique.

3. To suggest a technique that could improve urban damage assessment using the CCD technique with Sentinel-1 imagery.

Thesis Structure

This thesis includes 5 chapters. Chapter 1 presents the overview of the problems of disasters, both natural and human-caused disasters as well as the important role of remote sensing. This chapter also includes the overview of study areas and objectives of this study.

Chapter 2 provides a literature review which relates to change detection with spaceborne radar, concept of coherence, change detection and damage assessment with remote sensing data, and SAR techniques in change detection and damage assessment.

Chapter 3 describes the details of research methodology of this study which includes study areas, datasets, software, methodology workflow, and details of the processes.

Chapter 4 presents the experiment results of urban damage assessment of all study areas with 2 types of disasters including the 2023 earthquake in Turkey and the armed conflict between Russia and Ukraine.

Chapter 5 is the final chapter which includes a discussion and a conclusion of this study.

CHAPTER 2
LITERATURE REVIEWS

This chapter provides relevant literature which consists of change detection with spaceborne radar, concept of coherence, change detection and damage assessment with remote sensing data, and SAR techniques in change detection and damage assessment.

Urban Change Detection and Damage Assessment

The spaceborne radar antenna transmits a coherent signal toward the Earth and then the signal is backscattered by the Earth's surface before being detected by the same antenna. The SAR signal is complex. Each pixel of an image contains intensity and phase information. The intensity depends on the ground roughness, the soil moisture, the incidence angle and more. The phase information, expressed as an angle, depends on the optical path travelled by the radar wave along its round trip.

Two forms of change detection in repeat-pass SAR imagery can be considered to be coherence and incoherent change detection.

Incoherent change detection (ICD) identifies changes in the mean backscatter power of two scenes by comparing sample estimates of the mean backscatter power taken from the repeat-pass image pair. Typically, the sample estimates are obtained by spatially averaging the image pixel intensities (amplitude squared) over local regions in the image pair. The mean backscatter power of a scene is determined by the structural and dielectric properties of the scene, and thus may be used to detect changes in soil or vegetation moisture content or surface roughness.

Coherence change detection (CCD) compares the phase of two images for inconsistencies. This technique exploits the phase differences and the sensitivity of the SAR image speckle pattern. To detect whether a change has occurred, two images are taken of the same scene at different times. A change in scattering behaviour is observed via a reduction in the cross-correlation coefficient or coherence of the image pair. Two waves with a phase difference that remains constant over time are said to be

coherent or no change (Closson & Milisavljevic, 2017; Washaya, Balz, & Mohamadi, 2018).

Concept of Coherence

In a pulse radar system, coherence describes the phase relationships between the transmitted and the received pulses. Oscillations and electromagnetic waves are described as coherent if their phase relationships are constant.

The coherence image presents the confidence level of each pixel in the phase difference image. Coherence refers to a fixed relationship between waves in a beam of electromagnetic radiation. In SAR interferometry, coherence is used to describe systems that preserve the phase of the received signal. Coherence value can be estimated by means of the local coherence of an interferometric SAR image pair. The local coherence estimator is the complex cross-correlation coefficient of the couple estimated on a given window size, using Equation 1:

$$\gamma = \left| \frac{\frac{1}{N}\sum_{i=0}^{N} M_i S_i^*}{\sqrt{\frac{1}{N}\sum_{i=0}^{N} M_i M_i^* \frac{1}{N}\sum_{i=0}^{N} S_i S_i^*}} \right| \quad (1)$$

where N is the number of neighbouring pixels to be estimated, M and S are the complex signal of the master and slave images, respectively and * denotes the complex conjugate. γ is the resulting coherence (Washaya & Balz, 2018; Washaya et al., 2018). The coherence ranges from 0.0 (incoherent or total decorrelation, the interferometric phase is pure noise) to 1.0 (coherent, phase correlation is preserved). As a statistical value, it cannot provide quantitative measurements of the ground scatterers disturbances. However, a physical interpretation is that it represents the fraction of power scattered by unchanged parts of the scene (Bouaraba, Acheroy, & Closson, 2013). The coherence image serves as a measure of the quality of an interferogram and gives information about the surface type or shows when change has occurred in the image. Coherence imagery is able to detect centimetre scale changes in the scatterers distribution (Closson & Milisavljevic, 2017).

The coherence values are affected by many factors described as follows.

1. The local slope. Steep slopes oriented toward the satellite line of sight lead to low coherence).

2. The properties of the surface, for examples, vegetated or water surfaces have low coherence, urban built-up areas have high coherence.

3. The time span between the passes in an interferogram. Long lags lead to higher variations in scatterers distribution and hence to lower coherence.

4. The baseline, which is the distance between the positions of satellites. The perpendicular component is what matters for coherence purposes. Generally, the optimal baseline length is between 0 and 400 metres. Large baselines lead to low coherence.

5. The poor coregistration which is the process of lining up a master image and a slave image, covering the same area in a way that they fit exactly on top of each other.

Change Detection and Damage Assessment with Remote Sensing Data

Damage assessment is crucial for organizing the response to a disaster so that it can address the needs of the affected population and prevent any potential humanitarian crises. It is also an important step to support emergency response and reconstruction planning in a post-disaster. To obtain the spatial information on built and natural environments before and after the event occurred, several methods exist, such as field survey, airborne remote sensing, and satellite remote sensing. Because of its capability to cover a vast area in one acquisition time, satellite remote sensing has been a very powerful tool to monitor the condition of the earth surface. Satellite imagery can be very useful in post-disaster damage assessment if they are selected properly in terms of sensor type (optical or SAR), spatial resolution, repeat cycle of satellite, and the availability of pre-event images (Yamazaki & Matsuoka, 2007).

Products from both optical sensors and Synthetic Aperture Radar (SAR) are widely used in urban damage assessment. Each one has its advantages and disadvantages. Optical sensors can provide images to view the Earth's surface as the human eye does. High-resolution satellite imagery which has become available in the last few years, made satellite remote sensing more useful in disaster management since it can identify the damage status of individual buildings and infrastructures

without visiting the sites of disasters. However, the optical sensors can only function during daytime and cannot penetrate the clouds. On the other hand, SAR data are difficult to interpret, but they can operate both day and night in any weather conditions. Many researchers found that the capability of the combination of both optical sensors and SAR results in good accuracy.

Remote sensing technologies have been applied for post-disaster damage assessment by many researchers. Putri, Widyatmanti, and Umarhadi (2022) used the Sentinel-1 and Sentinel-2 data in building damage assessment of the earthquake that hit Lombok Island of Indonesia in 2018. They found that the fusion of SAR data from Sentinel-1 and optical data from Sentinel-2 provided the highest overall accuracy value compared to single data set models. Fakhri and Gkanatsios (2021) also used a combination of SAR and optical imagery to map and monitor changes in the urban environment due to war in the city of Mosul, Iraq which was captures by the Islamic State in June 2014. They also found that the results demonstrated the capability of combining both Sentinel-1and Sentinel-2 data for mapping the built-up area very accurately.

Optical and SAR imageries have their own advantages. Together they are very useful in urban change detection and damage assessment. However, since optical sensors operate under the conditions of sunlight and weather, using the combination of SAR and optical sensors is not always possible. Therefore, SAR can play a role in crisis management of disasters for promptly identifying damaged buildings and reasonably arranging rescue forces (Ge et al., 2020).

Many researchers have compared the performance of SAR and optical sensors in urban change detection and damage assessment. Aimaiti, Sanon, Koch, Baise, and Moaveni (2022) assessed the performance of Sentinel-1 and Sentinel-2 data for building damage assessment in Kyiv, the capital city of Ukraine, due to the ongoing war with Russia. They found that optical and SAR imagery have their own advantages with respect to damage recognition capabilities and outputs. Their comparison results showed that the SAR intensity-based analysis showed small to large scale damaged buildings, while optical texture-based analysis mainly showed the large-scale damaged buildings. Their comparison also showed that roof colour can influence the accuracy of the optical texture-based analysis, while both white and dark

roof damaged buildings were identified by the SAR intensity analysis. While Putri et al. (2022) found that the best result of building damage assessment produced by the combination of Sentinel-1 and Sentinel-2 data, they also found that the performance of optical data from Sentinel-2 was better than SAR data from Sentinel-1 in classifying building damage of the earthquake in Lombok Island of Indonesia in 2018.

SAR Techniques in Change Detection and Damage Assessment

Techniques to detect changes and damage in urban areas with remote sensing have been effectively used in a variety of applications. Due to the benefits of SAR technologies with the development of interpretation techniques, a variety of ways for SAR-based building damage assessment in disasters have been presented. These approaches range from methods applying both pre-event and post-event data to methods using only post-event data, depending on the data availability, resolution level, and acquisition mode. They also range from methods performing analysis in a block unit to methods performing analysis in a building unit, from methods based on intensity information to methods based on coherence or polarimetry information, and from methods exploring traditional physical relationships to methods exploring econometric relationships. All approaches have different advantages and disadvantages, the optimal solution in one case may not work well in another. There is no absolute optimum approach for all cases (Ge et al., 2020).

Coherence Change Detection

This section gives a review of studies on damage assessment based on coherence. Coherence change detection (CCD) is a technique that detects differences between pairs of SAR images. In this process, the estimated coherence between a pair of complex SAR images is calculated. Commonly, if the estimated coherence is high there is no change whereas low estimated coherence provides an indication of change (Damini, Mantle, & Davidson, 2013). The easiest way to obtain a reliable change map is to use one single pair of SAR images, with one single image before the event and one single image after the event. However, more than one pre/post-SAR image together can be used to overcome the effects of noise and other disturbances in SAR images, which could lead to inaccurate decisions while using one single SAR data pair (Mastro, Masiello, Serio, & Pepe, 2022).

The CCD technique has been used and studied by many researchers. Plank (2014) studies techniques focusing on multi-temporal SAR procedures for rapid damage assessment including interferometric coherence and intensity correlation and found that coherence is more sensitive to smaller changes on the ground than the SAR intensity correlation. Coherence is better suited to detect lower damage levels as well as to better differentiate between slightly damaged and still intact buildings.

Jendryke, Balz, and Liao (2016) used Interferometric Synthetic Aperture Radar (InSAR) coherence technique to generate a set of maps that showed the spreading of the urban build-up area and its changes within. Their maps give a good indication whether the area under observation has man-made structures. They also have the possibility to identify dynamics in the built-up environment.

Washaya and Balz (2018) studied on the urban areas affected by disasters including earthquake and a hurricane using the coherence characteristics of SAR images. They applied the CCD technique using Sentinel-1 imagery and concluded that the CCD technique is a useful method in measuring urban change in areas that have been affected by disasters. However, although the CCD technique can detect small changes, it is not a good indicator of the intensity of change. Furthermore, the technique is not very useful in vegetated areas, which are constantly unstable and can only be used in urban built-up areas. Balz, Washaya, and Jendryke (2018) applied the CCD technique to monitor urban growth in Shanghai. They also applied the CCD technique on urban damage detection in the Syrian war. They found that the CCD technique offers a way to identify even small changes in urban environments. As urban areas typically show coherence over long periods, sudden reduction in coherence can be a sign of significant changes on the ground. For non-urban areas, CCD is less suitable, as such areas often show a quick loss of coherence, hindering the identification of meaningful changes. Therefore, CCD can be used to monitor urbanization processes, focusing on the increase of coherence. We can also analysis decrease in coherence, monitoring changes and destruction of urban areas.

Guida et al. (2018) applied CCD technique on multiple interferometrically pre-processed SAR images to automatically detect potential damage to buildings and other physical structures caused by the seismic event. Their result indicated that the proposed methodology is able to perform damage detection with a good level of

accuracy, as most of the detected points of change are concentrated around highly damaged buildings.

Ge et al. (2020) reviewed SAR techniques on building damage assessment in disasters. Coherence information is more sensitive to minor ground changes than intensity information. When interferometric SAR image pairs are available with suitable temporal and spatial baselines, coherence can provide valuable information for identifying building damage, especially minor damage. The coherence difference has been exploited for discriminating between damaged and undamaged buildings.

ElGharbawi and Zarzoura (2021) used the CCD technique to identify the damage resulted by the industrial explosion in Beirut city of Lebanon that occurred on 4 August 2020. They utilized a SAR stack with one post event image and nine pre-event images to identify the natural robust pre-event correlation behaviour of each pixel and statistically classify the damaged pixels based on probability analysis. They combined phase coherence and amplitude correlation to estimate the damage probability of each pixel, then identify damaged regions based on three significance levels or damage probabilities.

Moreover, Boloorani, Darvishi, Weng, and Liu (2021) studied to identify urban areas damaged or destroyed by war in the city of Mosul in Iraq. Their study showed that Sentinel-1 data with CCD can be generally used to detect war-induced damage and can be used as a robust tool to provide reliable information for decision-makers to plan post-war reconstruction programs or other disaster control procedures.

CHAPTER 3
RESEARCH METHODOLOGY

This chapter provides the details of research methodology of this study which includes study areas, datasets, software, methodology workflow, and details of the processes.

Study Area

There are two type of study areas which affected by two different types of disasters. One is an earthquake which is one of the deadliest natural disasters. Another one is an armed conflict, a human-caused disaster. Both kind of these disasters occurred several times throughout the human history, and they were destructive and led to great loss and suffering in human life and seriously harmed urban infrastructure on an extreme scale. The details of the study areas are described as follows.

Study Areas of Turkey

Antakya, the capital city of Hatay province, the southernmost province of Turkey. It lies near the mouth of the Orontes River, about 19 kilometres northwest of the Syrian border. This city was built around 300 BC by a general of Alexander the Great, has survived several previous calamitous earthquakes (Britannica, 2023a). On 6 February 2023, the city was heavily damaged by two powerful earthquakes with their epicentre in Kahramanmaras. The earthquakes and aftershocks destroyed some of the historical sites including the Ulu Mosque which built in the 18th century and the Church of St Paul (Estrin, Harbage, Balaban, & Yilmazel, 2023). About 3,100 buildings collapsed, trapping residents, and killing more than 20,000 people in the city. The damage was so profound that officials estimated that 80% of the city's remaining buildings needed to be demolished (White, Gates, Leatherby, Reinhard, & Abraham, 2023).

Iskenderun, historically known as Alexandretta, is a city in Hatay Province located on the eastern shore of the Gulf of Iskenderun on the Mediterranean coast of Turkey (Britannica, 2023b). Iskenderun is one of the largest container ports in the Eastern Mediterranean region. Its total cargo turnover amounted to 67.6 million

tonnes in 2022 (EastFruit, 2023). The port of Iskenderun suffered severe structural damage with docks collapsing due to an earthquake. A severe fire from toppled containers also erupted at the port. Several new buildings and the Latin Catholic church collapsed. Many buildings became too dangerous to inhabit.

Adana, a large city of Adana province in south-central Turkey. It is situated in the plain of Cilicia, on the Seyhan River. Adana lies in the heart of Cilicia, which was once one of the most important regions of the classical world. Modern Adana is a centre for regional trade, healthcare, and public and private services. This city also affected by the earthquake. Multiple high-rise residential buildings were reduced to rubble. Though Adana was less affected by the earthquake than other cities, 13 of its buildings collapsed, 23 were badly damaged, 120 were moderately damaged, and more than a thousand required demolition (Kirac, 2023).

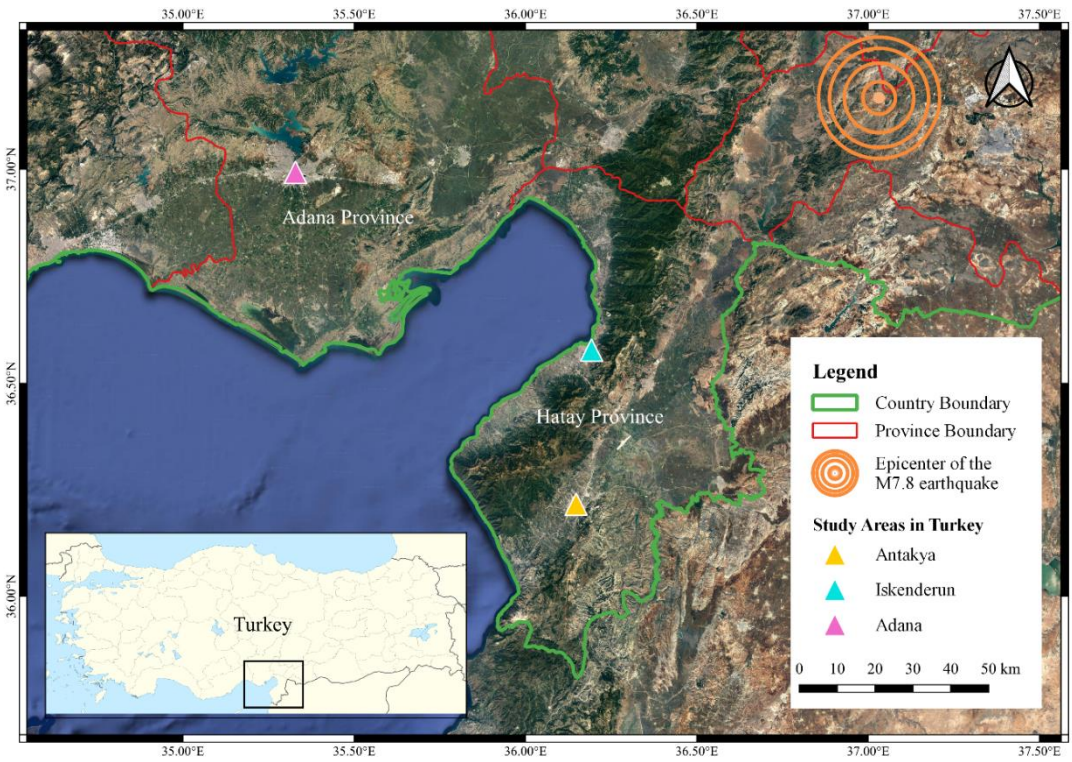

Figure 1 The study areas in Turkey.

Study Area of Ukraine

Mariupol, a port city on the north coast of the Sea of Azov at the mouth of the Kalmius River in Mariupol urban hromada (a basic unit of administrative division in Ukraine, similar to a municipality). It is located in Mariupol Raion (district) of Donetsk Oblast in the south-eastern Ukraine with an estimated population of 431,000 in 2021. The city occupies an area of 244 square kilometres including suburbs administered by the city council. Before the Russian invasion of Ukraine in 2022, it was the tenth-largest city in Ukraine. Mariupol played a key role in the industrialization of Ukraine, and was a centre for the grain trade, metallurgy, and heavy engineering. It is the base of a fishing fleet, and a dredged channel leads to the open sea. Mariupol has large iron- and steelworks and associated coke-chemical and machine-building works. The city also has other industries including ship repairing, fish canning, and flour milling. Following the invasion started on 24 February 2022, Mariupol was bombarded, and many buildings and infrastructure were destroyed or damaged (Britannica, 2022). The city was under siege for over a month. On 21 April 2022, Russian armed forces assumed full control over Mariupol, except for Azovstal plant area. Then, on 21 May 2022, Russia's defence ministry announced it had full control of Mariupol, following the evacuation of 1,908 defenders of the Azovstal plant there (Psaropoulos, 2022). United Nations Humans Rights assessed that up to 90 per cent of residential buildings were damaged or destroyed, as well as up to 60 percent of private houses. An estimated 350,000 people were forced to leave the city (Office of the High Commissioner United Nations Human Rights, 2022a).

Figure 2 The boundary of Mariupol urban hromada, Mariupol Raion, Donetsk Oblast, Ukraine.

Dataset

In this study, SAR imagery with VV polarisation acquired by Sentinel-1A satellite were used to analyse changes and damage in urban areas of the study areas. These data were provided by the European Space Agency (ESA) and were downloaded from the ESA Copernicus Open Access Hub website. The Sentinel-1A data are made available systematically and free of charge to all data users including the general public, scientific and commercial users. Sentinel-1A satellite is orbiting in Sun-synchronous near-polar orbit which has repeat cycle of 12 days and cycle length of 175 days (European Space Agency, 2012).

The acquisition mode of these data is Interferometric Wide (IW) swath which has a 250 kilometres swath and a 5 metres x 20 metres spatial resolution. These data are Level-1 Single Look Complex (SLC). This type of product consists of focused SAR data geo-referenced using orbit and attitude data from the satellite and

provided in zero-Doppler slant-range geometry. The products include a single look in each dimension using the full transmit signal bandwidth and consist of complex samples preserving the phase information (European Space Agency, n.d.-b). The data are available in dual polarisation VV and VH.

The IW swath mode is the main acquisition mode over land for Sentinel-1. It captures three sub-swaths using Terrain Observation with Progressive Scans SAR (TOPSAR). With the TOPSAR technique, in addition to steering the beam in range as in ScanSAR, the beam is also electronically steered from backward to forward in the azimuth direction for each burst, avoiding scalloping and resulting in homogeneous image quality throughout the swath. TOPSAR mode replaces the conventional ScanSAR mode, achieving the same coverage and resolution as ScanSAR, but with a nearly uniform Signal-to-Noise Ratio and Distributed Target Ambiguity Ratio (European Space Agency, n.d.-d). The IW SLC product contains one image per sub-swath and one per polarisation channel. Every IW SLC consists of 3 sub-swaths and each one of maximum 9 bursts or 10 bursts in some images as shown in the Figure 3.

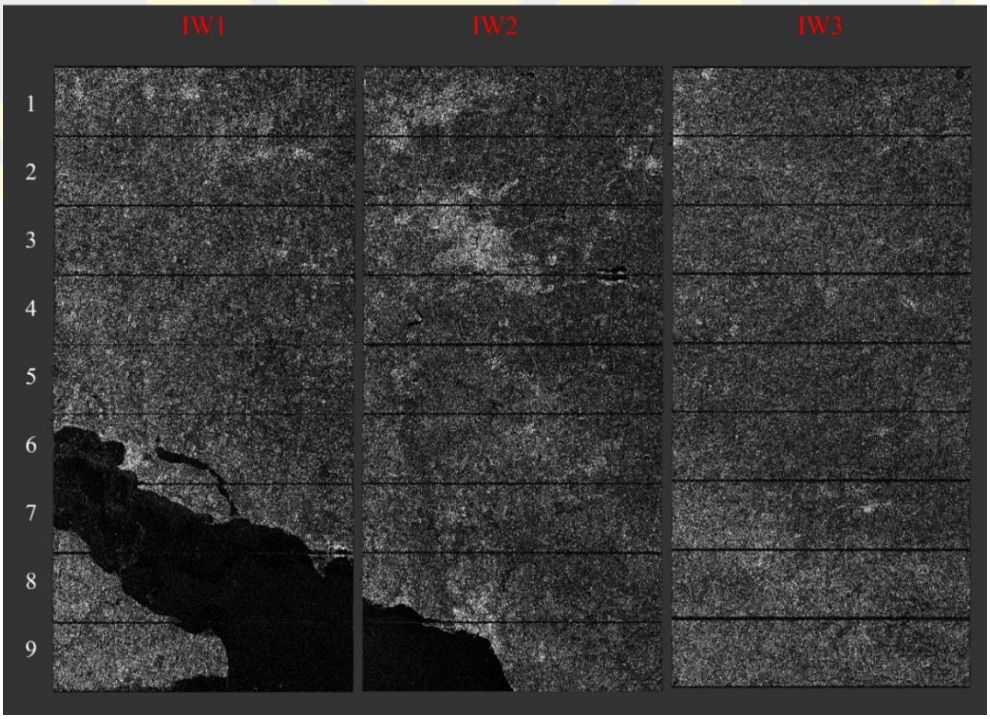

Figure 3 Sub-swaths (red) and bursts (white) of IW SLC products of Sentinel-1.

For each study area, images of three months before event were used. Since both events were in the same month, as Russia launched a special military operation in Ukraine on 24 February 2022 and the Turkey earthquake occurred on 6 February 2023, we decided to use the images from November 2021 for Ukraine and November 2022 for Turkey. These images of three months until the last image before the event represent late autumn and winter seasons and were used to create a single master correlation stack of each study area.

Dataset of Turkey

In case of the earthquake in Turkey, one image after the event of each study area was used because the earthquake occurred in a short period of time. The details of images used for study areas of the earthquake in Turkey are as follows.

Table 1 Details of SAR images for the study areas of the earthquake in Turkey.

Category	Date	Product description
Pre-event	5 November 2022 17 November 2022 29 November 2022 11 December 2022 23 December 2022 4 January 2023 16 January 2023 28 January 2023	Satellite: Sentinel-1A Instrument: SAR (C-band) Mode: IW Pass direction: Ascending Relative orbit number: 14 Slice number: 7-8
Post event	9 February 2023	

The study areas of Antakya and Iskenderun are located on the same coverage area of the same image, which is from relative orbit number 14, slice number 7, while Adana is located on the edges of both slice number 7 and 8 as shown in Figure 4. In this case, images of 2 coverage areas were assembled before doing further processes in the study area of Adana.

Figure 4 The coverage of SAR images for the study areas of the earthquake in Turkey.

Dataset of Ukraine

In case of the conflict between Russia and Ukraine in Mariupol, the event did not occur in a short period of time, but it lasted for a few months. Since the invasion began on 24 February 2022 until Russia claimed to have full control of Mariupol on 21 May 2022, multiple SAR images after 24 February 2022 were used to be post event images for damage assessment of the urban area throughout that period of time. The details of images used for study area of Mariupol are as follows.

Table 2 Details of SAR images for the study areas of Mariupol.

Category	Date	Product description
Pre-event	4 November 2021 16 November 2021 28 November 2021 10 December 2021 22 December 2021 3 January 2022 15 January 2022 27 January 2022 8 February 2022 20 February 2022	Satellite: Sentinel-1A Instrument: SAR (C-band) Mode: IW Pass direction: Descending Relative orbit number: 94 Slice number: 6
Post event	4 March 2022 16 March 2022 28 March 2022 9 April 2022 21 April 2022 3 May 2022 15 May 2022 27 May 2022 8 June 2022 20 June 2022	Satellite: Sentinel-1A Instrument: SAR (C-band) Mode: IW Pass direction: Descending Relative orbit number: 94 Slice number: 7

The data from November 2021 to April 2022 are from the relative orbit number 94 and slice number 6 while the data from May to June 2022 are from the relative orbit number 94 and slice number 7 as shown in Figure 5, because since May

2022 the slice number 6 has not covered the study area of Mariupol. Its coverage area has moved to the north, as a result, Mariupol has been in the coverage area of slice 7 instead.

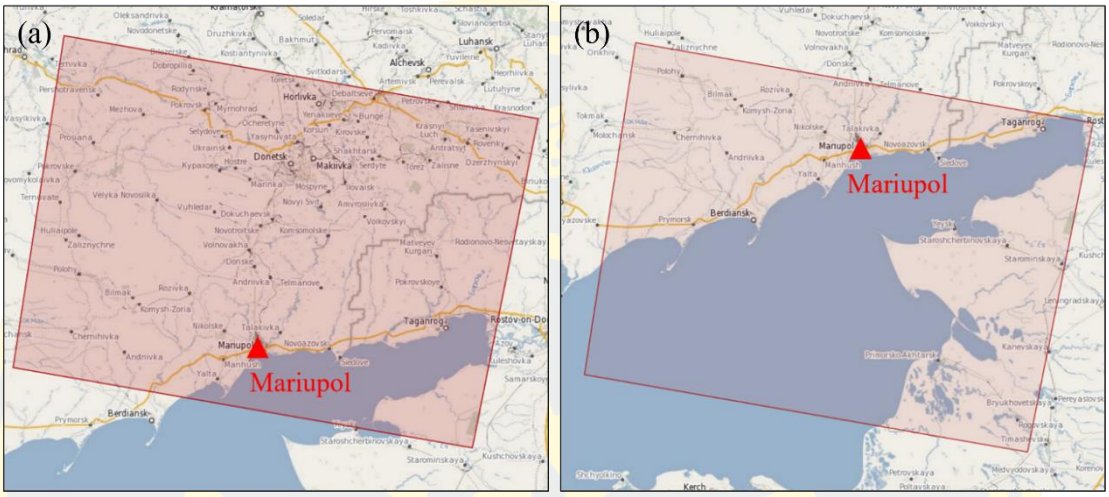

Figure 5 The coverage of SAR images for the study areas of Mariupol (a) from November 2021 to April 2022 (b) from May to June 2022.

Software

A software named SNAP was used to process SAR data acquired by Sentinel-1A. SNAP or The Sentinel Application Platform, a freeware developed by Brockmann Consult, Skywatch, Sensar and C-S (European Space Agency, n.d.-e). SNAP provides users with the tools they need to process satellite data with open toolbox that can be used for processing data products from several satellite missions such as Sentinel-1, Sentinel-2 and Sentinel-3, as well as ESA's SMOS mission, and Third Party Missions (European Space Agency, 2020). In this study, we used SNAP version 9.0.0, released on 29 June 2022 with Sentinel-1 Toolbox which can support most SAR missions with updates to the Sentinel-1 format.

Another software used in this study is QGIS, a free and open-source geographic information system (GIS) developed by a community of contributors. This software allows users to create, edit, visualize, and analyse spatial information. In this study, we use QGIS to visualise and analyse data that generated from SNAP, and we

also used it to create and export data as graphical maps and histograms of result images. QGIS that we used in this study was QGIS version 3.28 LTR, released on 21 October 2022.

Methodology Workflow

The basic idea is to identify the natural statistical behaviour of each pixel before the hazardous event and minimize the impact of atmospheric phase disturbances by using a stack of pre-event coherence images and generating a master coherence image before the event, a series of images can be analysed to get more reliable pre-event master coherence image. Then, compare the post-event behaviour of a pixel with its estimated natural behaviour from the pre-event master coherence image to determine whether there is a change.

In order to create a stack of pre-event coherence images, we had to generate a coherence image of each consecutive image pair, for instance, coherence image of 4 and 16 November, 16 and 28 November, 28 November and 10 December, 10 and 22 December, and so on. The time interval of 2 images of each pair is 12 days due to a repeat cycle of Sentinel-1A. Then, we generated an average coherence image from those coherence images in the stack to be a master pre-event coherence image as a reference.

After we created the master pre-event coherence image, the next step was to create a post event coherence image and compare the coherence value of the average pre-event coherence image and the post event coherence image. In this step, we used the log ratio which is the logarithm with base 10 or common logarithm, to calculate changes of coherence value before and after event. The log ratio of coherence value is calculated as Equation 2:

$$I_{ratio} = \log\left(\frac{I_{post}}{I_{pre}}\right) \tag{2}$$

where I_{post} is the post event coherence image and I_{pre} is the average pre-event coherence image. The log ratio is an effect-size statistics, not a significance statistic. Therefore, the log ratio can represent how large the difference of coherence value

between before and after the event. By taking the log-ratio, the distribution is more likely to behave like a normal distribution or Gaussian distribution and the value of log ratio are positive and negative (Swamy, 2015). In this study, negative log ratio value indicates decreasing in coherence value and positive log ratio value indicates increasing in coherence value, while log ratio value of zero means no change. The workflow overview of this study is shown in Figure 6.

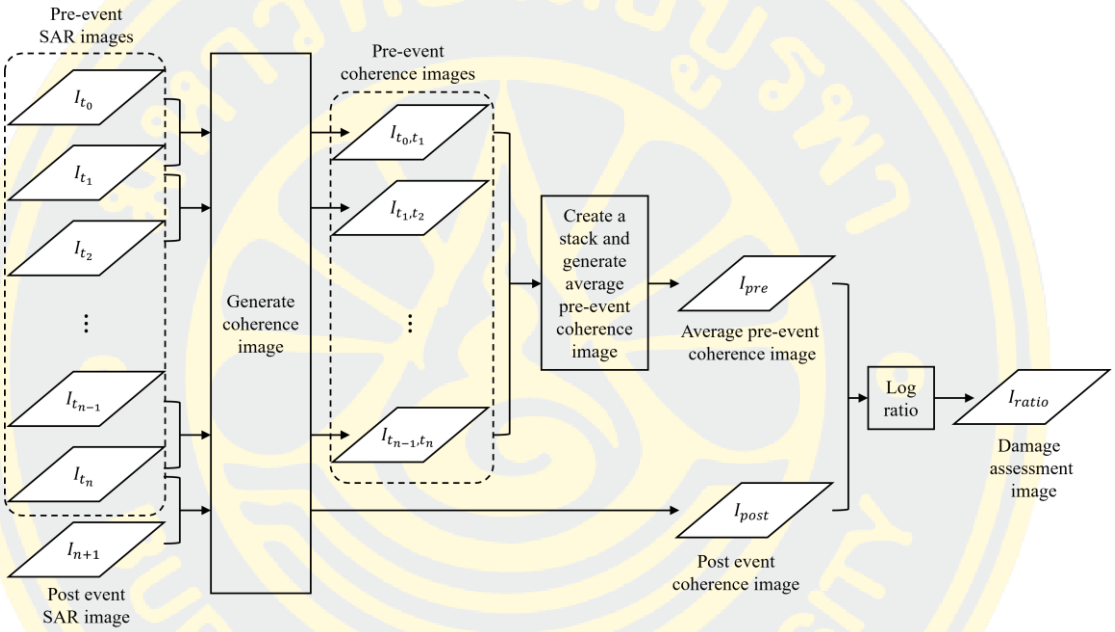

Figure 6 The workflow overview of the study.

Coherence Image Generation

We generated coherence images of pairs of images for each study area in a period of time from three months before an event until the day of the first image after that event occurred. Each pair of images consisted of two SAR images with 12 days of time interval. The process of coherence image generation for a pair of SAR images from using Sentinel-1A images with SNAP version 9.0.0 includes the following steps: splitting an image for a study area, applying orbit information, coregistration, coherence estimation, TOPS Deburst, terrain correction, and subset generation for a study area as shown in Figure 7.

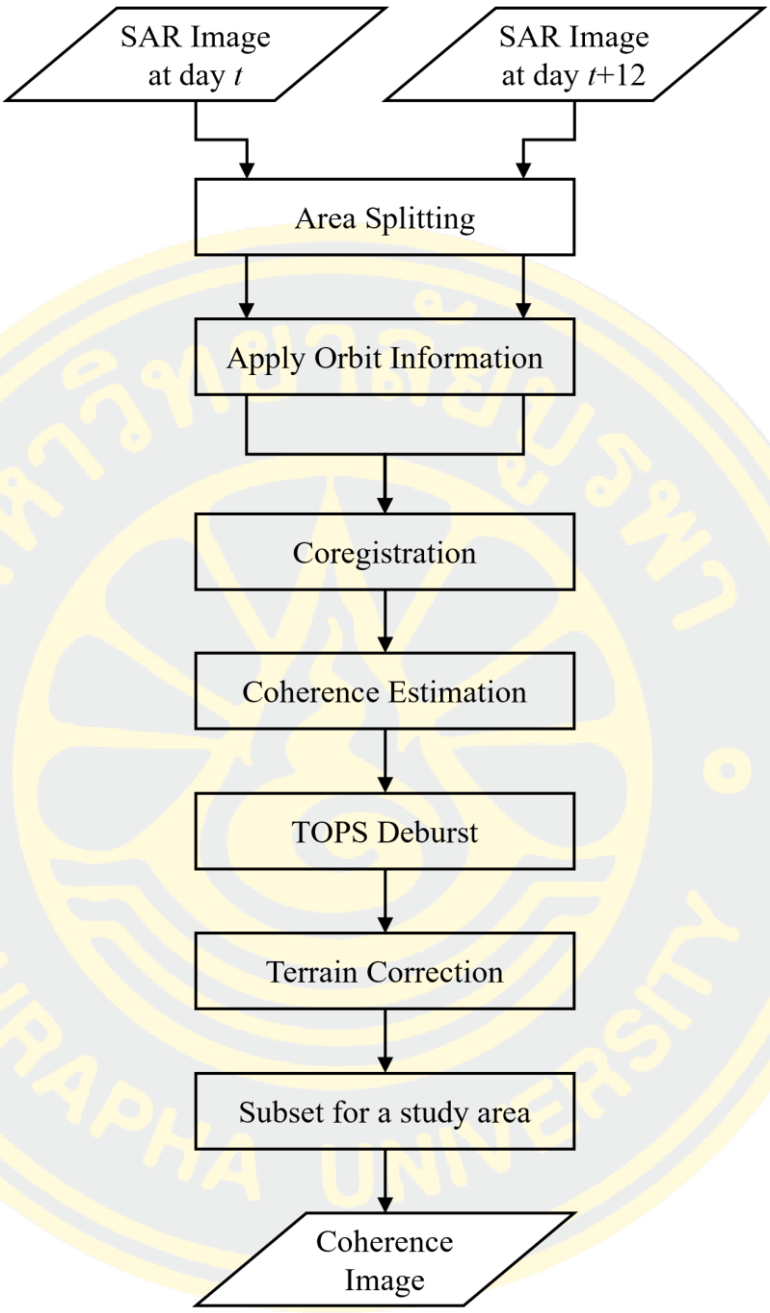

Figure 7 The workflow of coherence image generation.

Area Splitting

The datasets used in this study are the Interferometric Wide (IW) swath mode and Single Look Complex (SLC) type. Each sub-swath image consists of a series of bursts, where each burst has been processed as a separate SLC image. The individually focused complex burst images are included, in azimuth-time order, into a single sub-swath image with black-fill demarcation in between. There is sufficient overlap between adjacent bursts and between sub-swaths to ensure continuous coverage of the ground as provided in Ground Range Detected (GRD) products. The images for all bursts in all sub-swaths are resampled to a common pixel spacing grid in range and azimuth while preserving the phase information (European Space Agency, n.d.-d).

To reduce the data to a study area, we selected only sub-swath and bursts that cover the study area which are required for the analysis by using the S-1 TOPS Split operator (under *Rader > Sentinel-1 TOPS*) in SNAP.

In this step, we selected different sub-swaths and bursts for different study areas. For Turkey, the study areas are the cities of Antakya and Iskenderun in Hatay province which are located in the same coverage area of SAR images with relative orbit number 14 and slice number 7. Another study area of Turkey is the city of Adana in Adana province which located in SAR images with relative orbit number 14 and slice number 7 and 8. In this case, we assembled 2 images of slice number 7 and 8 with the same date together to make them as one image by using the S-1 Slice Assembly operator (under *Radar > Sentinel-1 TOPS*). The assembled image combined sub-swaths and bursts of both images together. As a result, each sub-swath of the assembled image contained 18 bursts, or 19 bursts. We selected sub-swath IW1 bursts 9 to 11 to be split for the study area of Adana and sub-swath IW2 bursts 5 to 7 to be split for the study are of Antakya and Iskenderun as shown in Figure 8.

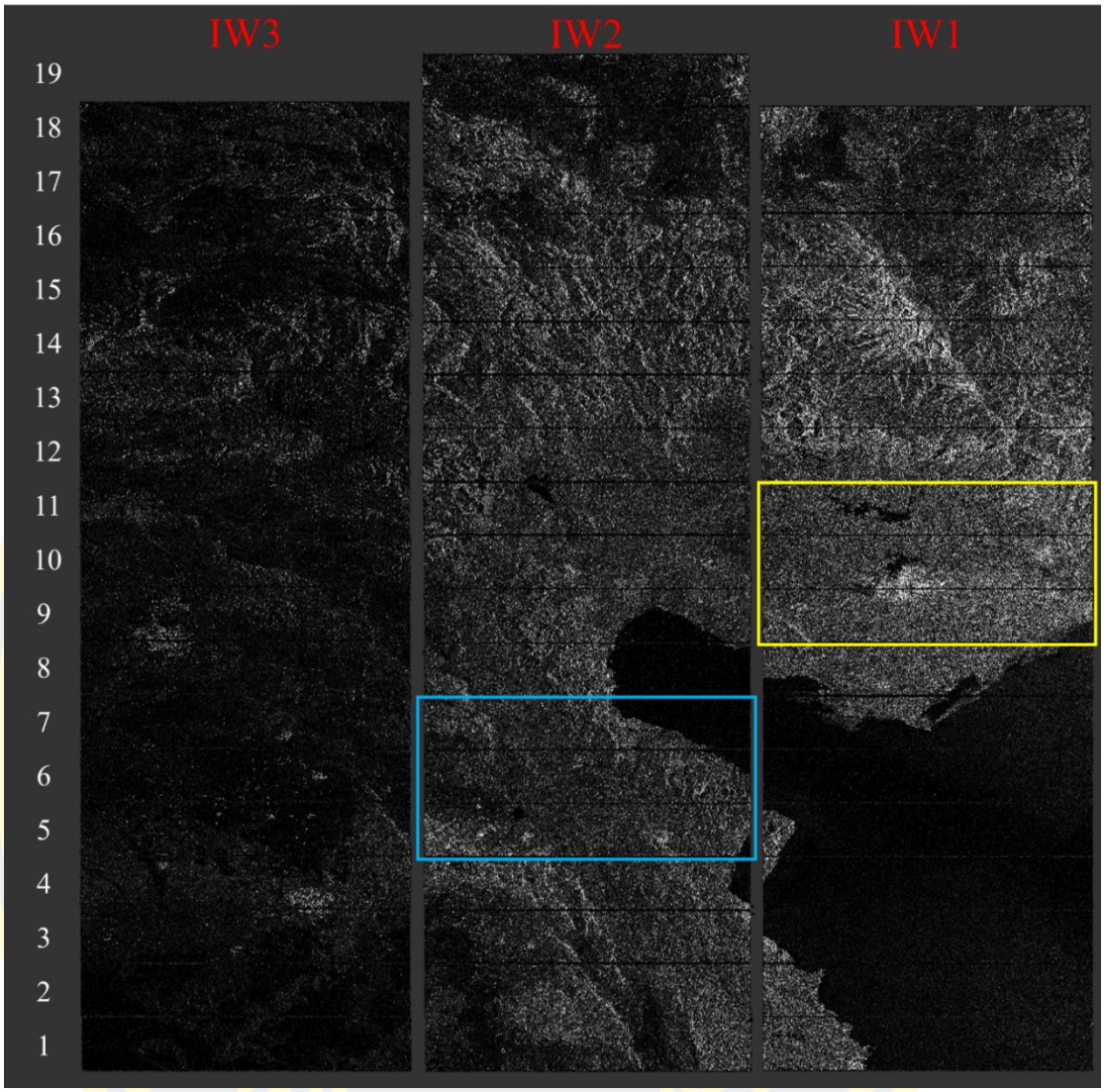

Figure 8 Sub-swaths (red) and bursts (white) of an assembled image of the study areas of Turkey, blue box for Antakya and Iskenderun, yellow box for Adana.

For Mariupol, the study area is located in sub-swath IW2 and bursts 8 and 9 for SAR images from November 2021 to April 2022 with relative orbit number 94 and slice number 6. For SAR images from May to June 2022 with relative orbit number 94 and slice number 7, the study area is located in sub-swath IW2 and bursts 2 and 3 as shown in Figure 9.

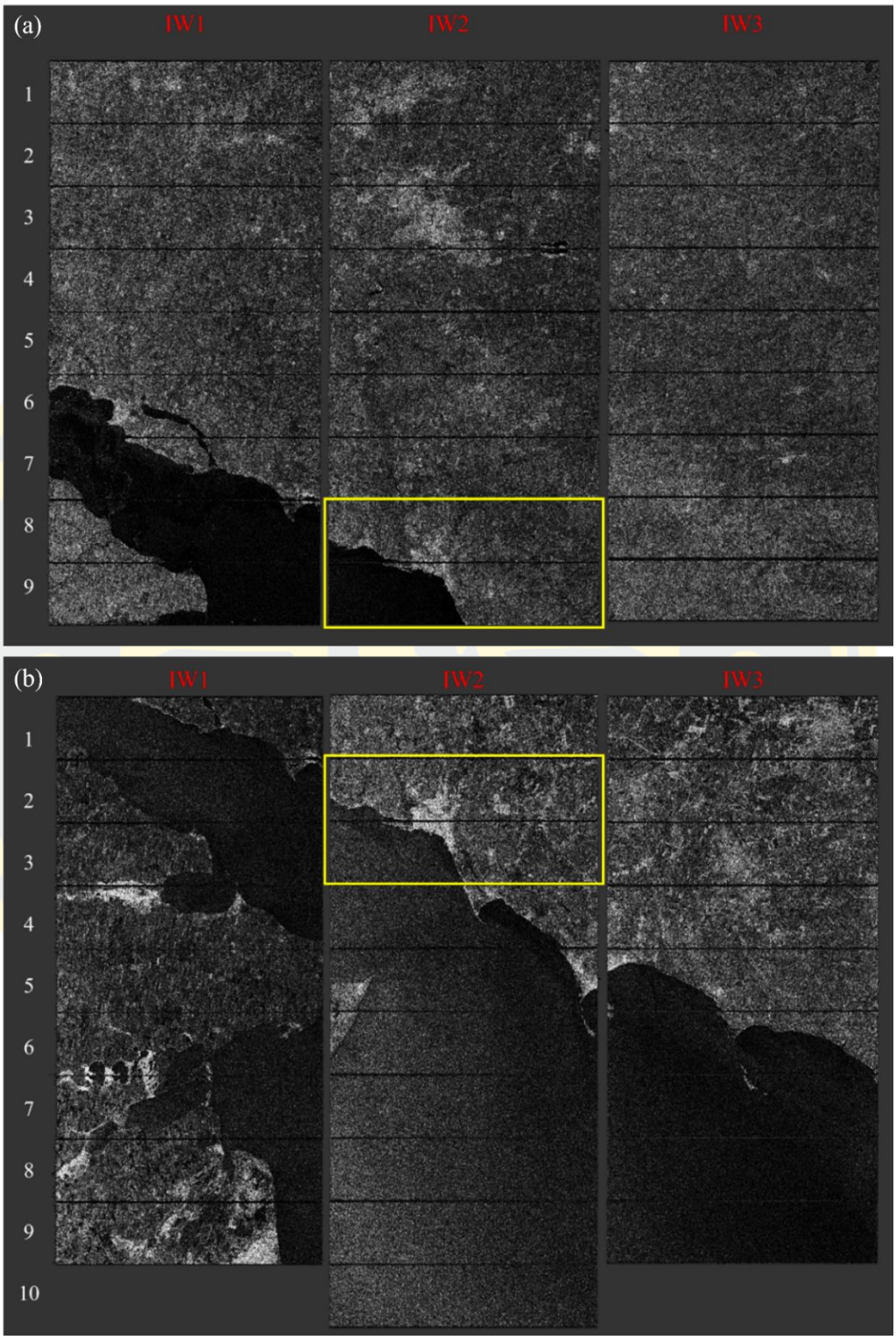

Figure 9 Sub-swaths (red) and bursts (white) of an image of the study area of Mariupol in yellow box (a) relative orbit number 94 and slice number 6 (b) relative orbit number 94 and slice number 7.

Applying Orbit Information

Orbit auxiliary data contain information about the position of the satellite during the acquisition of SAR data. They are automatically downloaded for Sentinel-1 products by SNAP and added to its metadata. To applying orbit information, we used the Apply Orbit File (under the menu point *Radar*) operator with default settings.

Coregistration

To exploit the phase difference of the acquisitions, we had to create a stack containing a pair of images which were already split for a study area and applied orbit information. Image coregistration is the alignment of master and slave images, the pixels of the slave images correspond to those of the master and represent an identical area. It makes use of image statistics to align both products at sub-pixel accuracy. To do this, we used an operator called S-1 Back Geocoding (under *Radar* > *Coregistration* > *Sentinel-1 TOPS Coregistration*). This operator coregisters the two split products based on the orbit information added in the previous step and information from a digital elevation model (DEM) which is downloaded by SNAP. In this study, we used SRTM 1Sec HGT (AutoDownload) in the Back-Geocoding tab as shown in Figure 10. The Shuttle Radar Topography Mission (SRTM) is only available between 60 degrees north latitude and 54 degrees south latitude which can be used for the study areas (NASA, 2023).

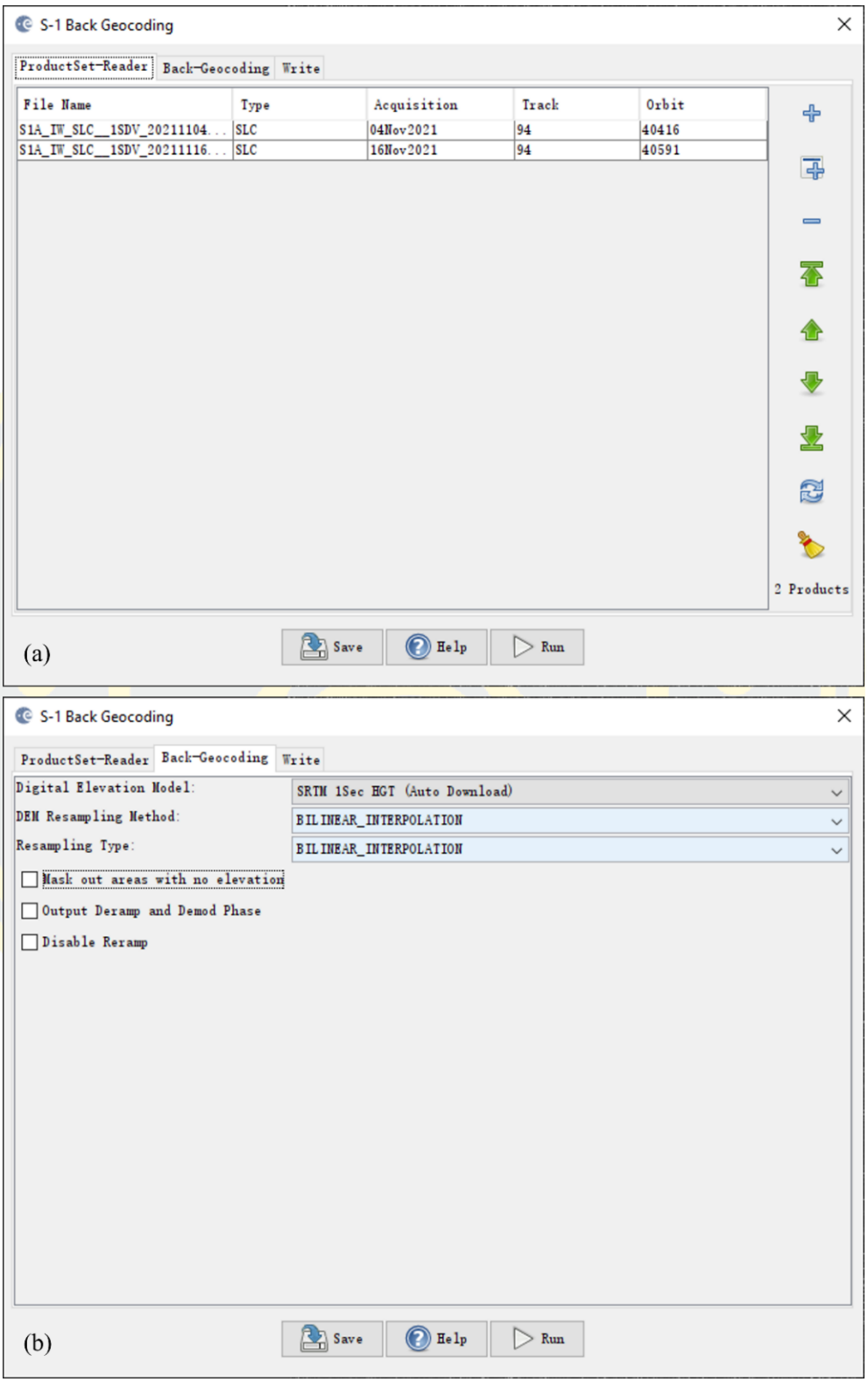

Figure 10 The S-1 Back Geocoding operator (a) a pair of images to be coregistered (b) settings of the S-1 Back Geocoding operator.

After those 2 images were coregistered in a stack by the S-1 Back Geocoding operator, we increased their quality of the coregistration by applying the S-1 Enhanced Spectral Diversity (ESD) operator (under *Radar* > *Coregistration* > *Sentinel-1 TOPS Coregistration*) on the stack using default settings. Then, we got the coregistered product of the intensity bands of both products, this operator is only needed when a split images are more than one burst. In this study, every image of each study area contains more than one burst.

Coherence Estimation

Coherence is calculated as a separate raster band and shows how similar each pixel is between two images in a scale from 0 to 1 (European Space Agency, n.d.-c). Areas that appear bright indicate high coherence. On the other hand, areas that appear dark indicate low coherence. To compute the coherence bands of a pair of images, we applied the Coherence Estimation operator (under *Radar* > *Interferometric* > *Products*) to the stack that was generated after Back Geocoding and ESD in the previous step. The Coherence Estimation operator produced a coherence band in the output which calculated based on a window of 10x3 pixels in range and azimuth direction as default settings of this operator as shown in Figure 11.

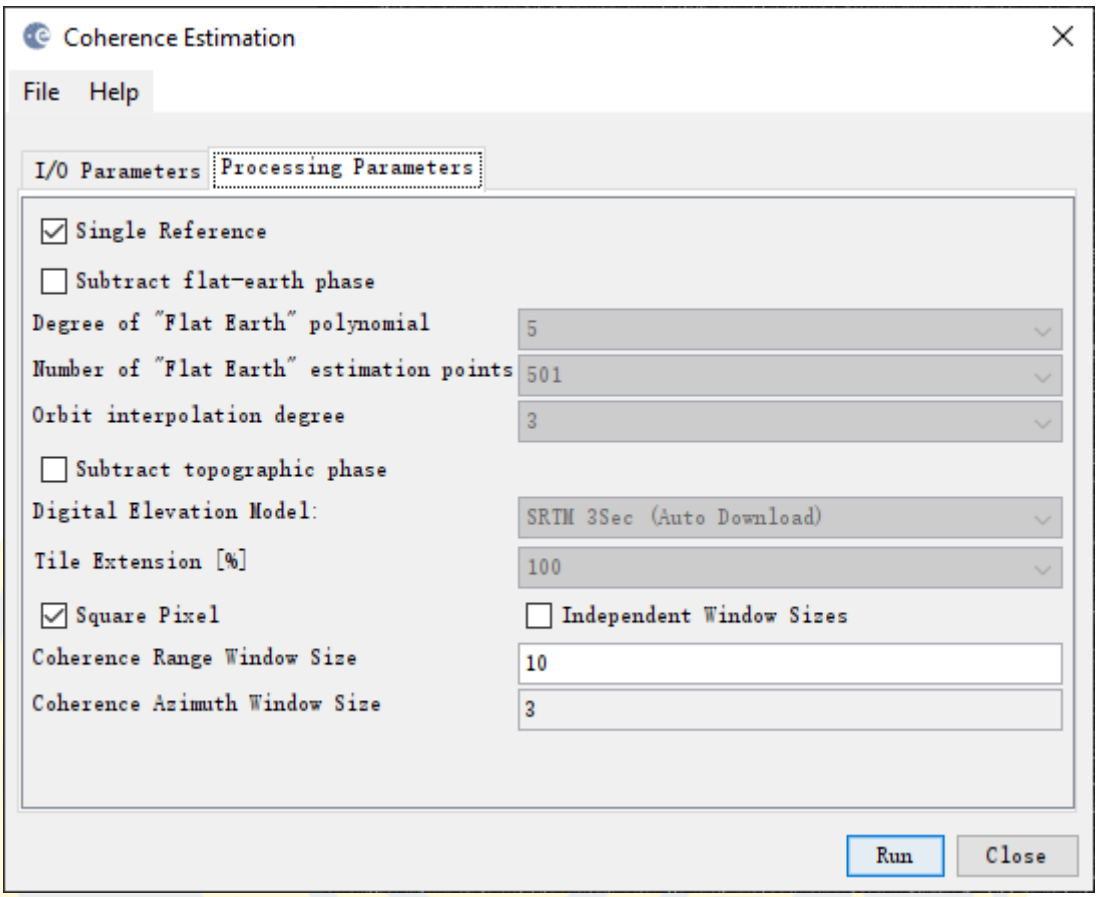

Figure 11 The Coherence Estimation operator.

TOPS Deburst

This process is to remove the seamlines or the black space between the bursts. Since we used more than one burst for each study area, we had to apply the S-1 TOPS Deburst operator (under *Radar > Sentinel-1 TOPS*) to the coherence product generated in the previous step using default settings. The output contains the same bands as the input, but with merged bursts according to their zero Doppler time.

Terrain Correction

After we generated a coherence image and removed the seamlines between the bursts, the next step was to apply the terrain correction process. This process is to geocode the image by correcting SAR geometric distortions using a digital elevation model (DEM) and producing a map projected product. Geocoding converts an image

from slant range or ground range geometry into a map coordinate system. Terrain geocoding involves using a DEM to correct for inherent geometric distortions.

To do this, we applied the Range Doppler Terrain Correction operator (under *Radar* > *Geometric* > *Terrain Correction*). In the Processing Parameters tab, we used SRTM 1Sec HGT (AutoDownload) as input DEM as same as the S-1 Back Geocoding operator in the Coregistration step and used Pixel Spacing at 10 metres for all coherence images as shown in Figure 12.

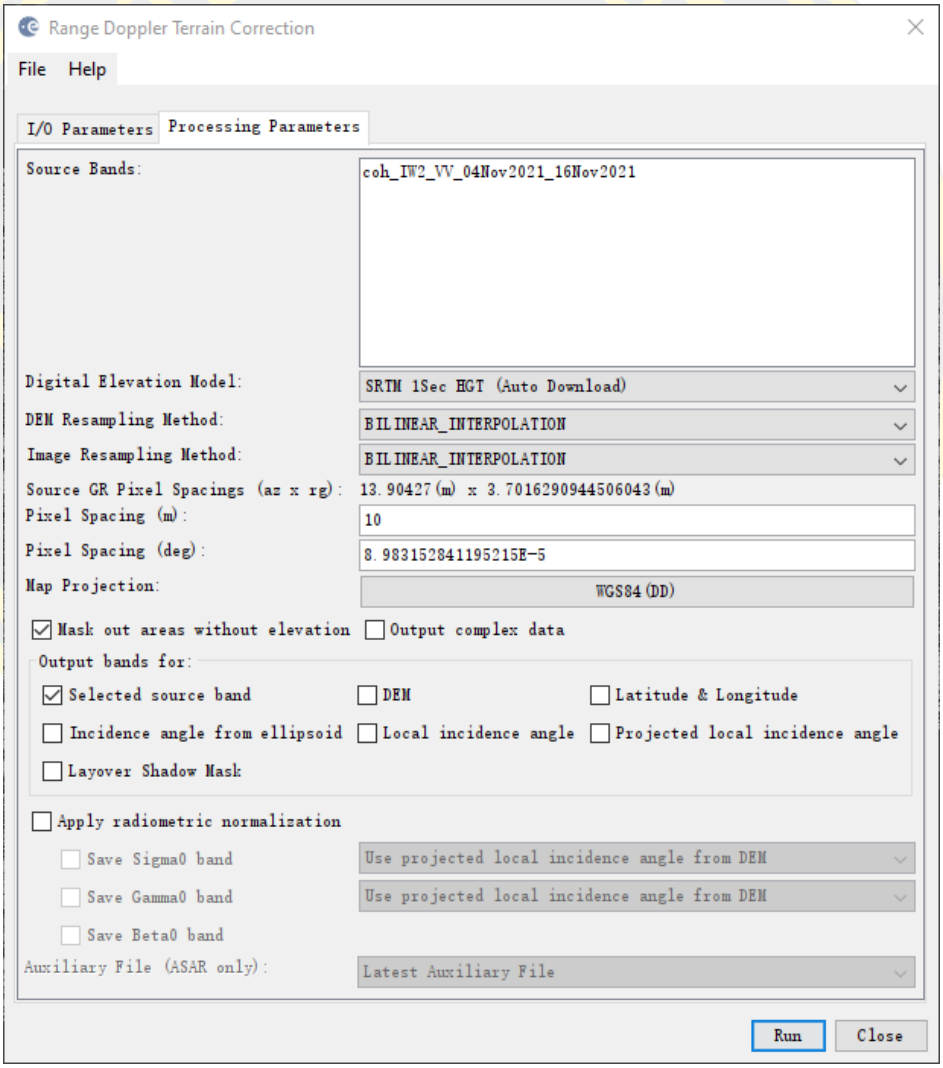

Figure 12 The Range Doppler Terrain Correction operator.

Subset for a Study Area

The selected bursts that we applied by the S-1 TOPS Split operator and continued to the Terrain Correction process were cover a larger area than a study area which we required for further analysis. In this step, we generated a subset for a study area by using the Subset operator (under *Raster*).

In this study, we used different geo coordinates for each study area to generate subsets of coherence images, since we need to focus coherence value only in urban areas. The coordinates used to create a subset of each study area are shown in Table 3.

Table 3 Geo coordinates of the study areas to create subsets.

Study areas	**North latitude bound**	**South latitude bond**	**West longitude bond**	**East longitude bond**
Antakya	36.28	36.16	36.10	36.23
Iskenderun	36.62	36.53	36.07	36.22
Adana	37.07	36.95	35.18	35.45
Mariupol	47.22	46.98	37.43	37.74

After we finished this process, we got a coherence image of a pair of SAR images. Then, we repeated all steps of the coherence image generation for each consecutive image pair. Those coherence images then were used to generate an average pre-event coherence image to be compared with a post event coherence image in further steps.

For the study areas of Turkey including the cities of Antakya and Iskenderun in Hatay province and Adana in Adana province, we created 7 pre-event coherence images for each city from 5 November 2022 to 28 January 2023 and one post event coherence image. The total number of coherence images generated for 3 study areas of Turkey is 24 as details in Table 4.

Table 4 List of coherence images per each study area of Turkey.

Number	Coherence maps	Catgegory
1	5 November 2022 and 17 November 2022	
2	17 November 2022 and 29 November 2022	
3	29 November 2022 and 11 December 2022	
4	11 December 2022 and 23 December 2022	Pre-event
5	23 December 2022 and 4 January 2023	
6	4 January 2023 and 16 January 2023	
7	16 January 2023 and 28 January 2023	
8	28 January 2023 and 9 February 2023	Post event

For the study area of Mariupol in Ukraine, we created 9 pre-event coherence images from 4 November 2021 to 20 February 2022 and 10 post event coherence images as details in Table 5.

Table 5 List of coherence images of Mariupol.

Number	Coherence maps	Category
1	4 November 2021 and 16 November 2021	
2	16 November 2021 and 28 November 2021	
3	28 November 2021 and 10 December 2021	
4	10 December 2021 and 22 December 2021	
5	22 December 2021 and 3 January 2022	Pre-event
6	3 January 2022 and 15 January 2022	
7	15 January 2022 and 27 January 2022	
8	27 January 2022 and 8 February 2022	
9	8 February 2022 and 20 February 2022	

Table 5 (continue)

Number	Coherence maps	Category
10	20 February 2022 and 4 March 2022	Post event
11	4 March 2022 and 16 March 2022	
12	16 March 2022 and 28 March 2022	
13	28 March 2022 and 9 April 2022	
14	9 April 2022 and 21 April 2022	
15	21 April 2022 and 3 May 2022	
16	3 May 2022 and 15 May 2022	
17	15 May 2022 and 27 May 2022	
18	27 May 2022 and 8 June 2022	
19	8 June 2022 and 20 June 2022	

Average Pre-event Coherence Image Generation

After we generated each coherence image from each pair of SAR images which are in the period of 3 months before an event, we generated an average pre-event coherence image to be the master coherence image and the representative coherence image for all pre-event coherence images. This step can minimize the impact of atmospheric phase disturbances, weather, and the effect of noise and other disturbances in SAR images which could lead to inaccurate decisions while using one single pre-event coherence image (Mastro et al., 2022).

To generate a reliable pre-event master coherence image, all pre-event coherence images were stacked in chronological order and used the last coherence image before an event to be the reference or the master of the stack. This process, we used the Create Stack operation (under *Radar* > *Coregistration* > *Stack Tools*) and we used Product Geolocation as initial offset method. In this study, we included pre-event and post event coherence images in the same stack for each study area for further processes.

After all pre-event coherence images were aligned in a single stack, we calculated average coherence for every pixel of images by using the Band Maths

operator. In this operator, there is The Band Maths Expression Editor which provides a convenient way to construct maths expressions with C syntax from various data sources, such as bands, tie-point grids and flag values. We can combine these data sources by several comparison, arithmetic, logical and binary operators or use them as arguments for mathematical functions (European Space Agency, n.d.-a). In this study, we used average function to calculate average coherence for all pre-event coherence images as shown in Figure 13.

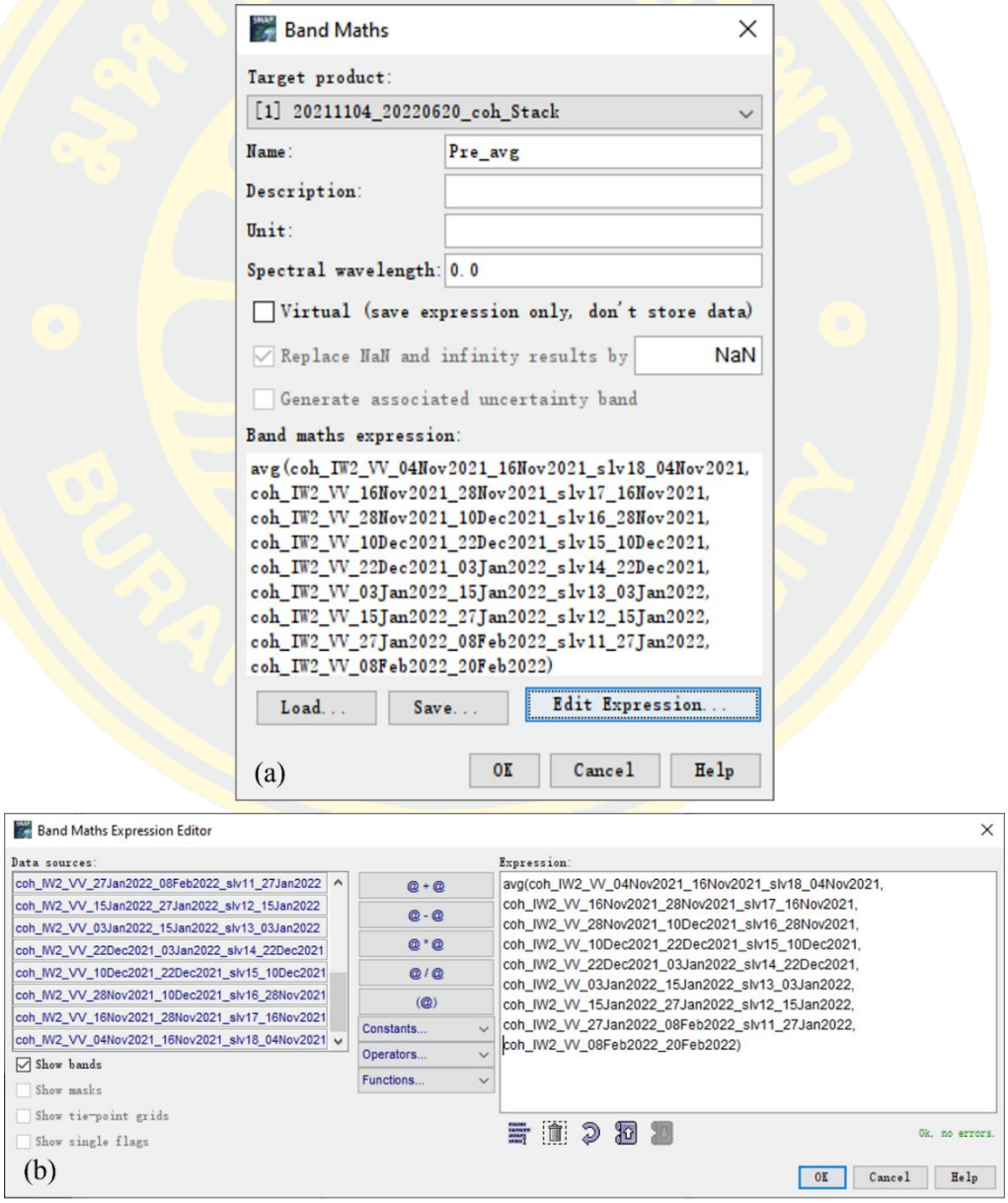

Figure 13 (a) The Band Maths operator (b) The Band Maths Expression Editor.

After we executed the Band Maths operator, we got an average pre-event coherence image as a new band in the stack to be processed in the next step.

Change Detection

This step is to detect the changes between the two coherence images which are the average pre-event coherence image and post event coherence image. This process can be done by two methods. The first one is to use the Band Maths operator and the second one is to use the Change Detection operator.

To use the Band Maths operator mentioned in the previous step, we selected the logarithm with base 10 function or common logarithm function in the Band Maths Expression Editor to generate log ratio image of post event coherence image and average pre-event coherence image. Since the stack of coherence images that we created in the previous step included all pre-event coherence images, post event images, and average pre-event coherence image, we applied the Band Maths operator to this stack. Then, we selected only a post event coherence image that we needed and the average pre-event coherence image as data sources to be calculated by the logarithm with base 10 as shown in Figure 14.

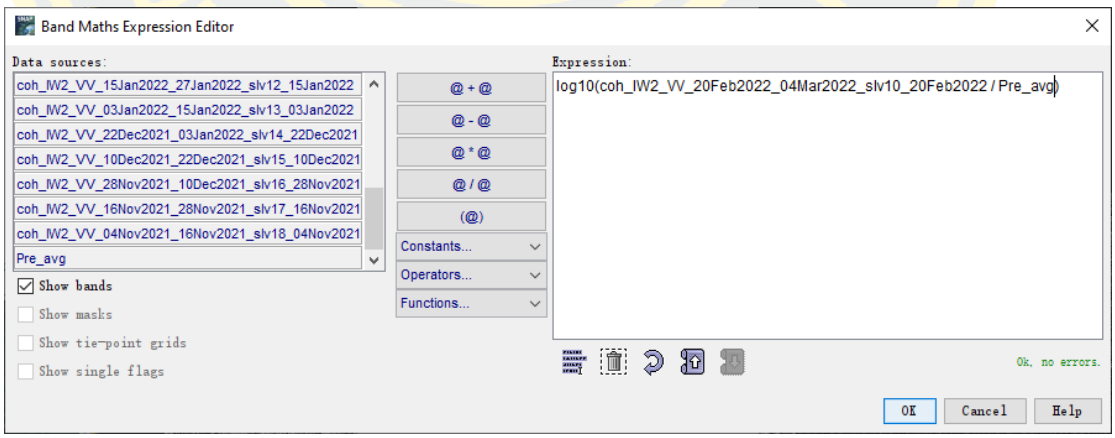

Figure 14 The expression of the Band Maths Expression Editor for the log ratio.

After we executed the Band Maths operator, we got a new band of a log ratio image for coherence change detection as a new band in the stack to be processed in the next step.

Using the Change Detection operator is another method to generate a log ratio image for coherence change detection, we applied the Change Detection operator (under *Radar* > *SAR Application*) to the stack of pre-event coherence images, post event images, and average pre-event coherence image. Then we selected a post event coherence image that we needed and the average pre-event coherence image as source bands and we selected the Output Log Ratio checkbox to make this operator calculate by using the logarithm with base 10. The output of this method contained a log ratio band and a change detection band. However, we used only the log ratio band in this study, so we let parameters of mask upper threshold and mask lower threshold be as default.

After we executed the Change Detection operator, we got a new product that contained a log ratio image which is the same as log ratio image generated by the Band Maths operator. As a result, these log ratio images of the post event coherence image and the average pre-event coherence image are the coherence change images of this study, which we used for urban damage assessment for the study areas.

Preparing Data for Analysis

In this step, we exported average pre-event coherence images, post event coherence images, and log ratio images of all study areas as the GeoTIFF format from SNAP. Then, we used QGIS to visualize, edit, and analyse those data for each study area. Although, we generated a subset for each study area in the previous step, yet we needed to generate subsets of urban areas for each study area as we needed to focus on urban areas with medium and high density of buildings. To do this, we create polygons of urban areas for each study area and used the Clip Raster by Mask Layer operator (under *Raster* > *Extraction*) in QGIS to clip average pre-event coherence images, post coherence event images and log ratio images by the polygons of urban areas for each study area. Finally, we got average pre-events coherence images, post event coherence images of urban areas for the study areas which we used for further analysis.

CHAPTER 4
RESULTS

This chapter consists of results from our experiments with two disasters including the 2023 earthquake in Turkey and the armed conflict between Russia and Ukraine. It also contains examples of comparison for pre-event images and post event images from Google Earth, and the results from this study.

Turkey

The results of each study area including Antakya and Iskenderun in Hatay province and Anada in Adana province, consist of an average pre-event coherence image, a post event coherence image, a log ratio image, a log ratio with Google Earth overlay image, and their histograms.

Antakya

We created the area of interest for urban areas of Antakya as shown in Figure 15 and the results of the area of interest as shown in Figure 16 with histograms shown in Figure 17.

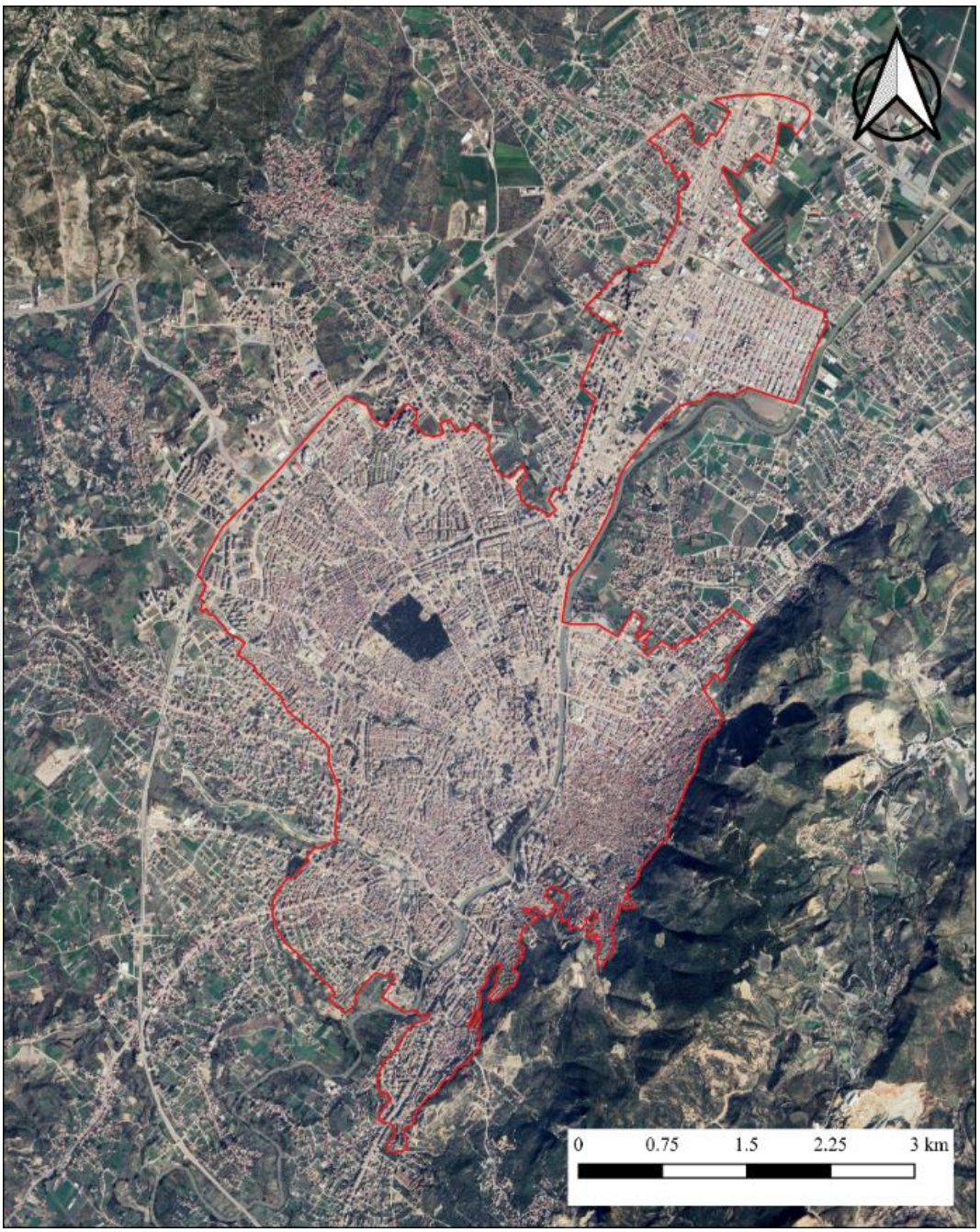

Figure 15 The area of interest for urban areas of Antakya.

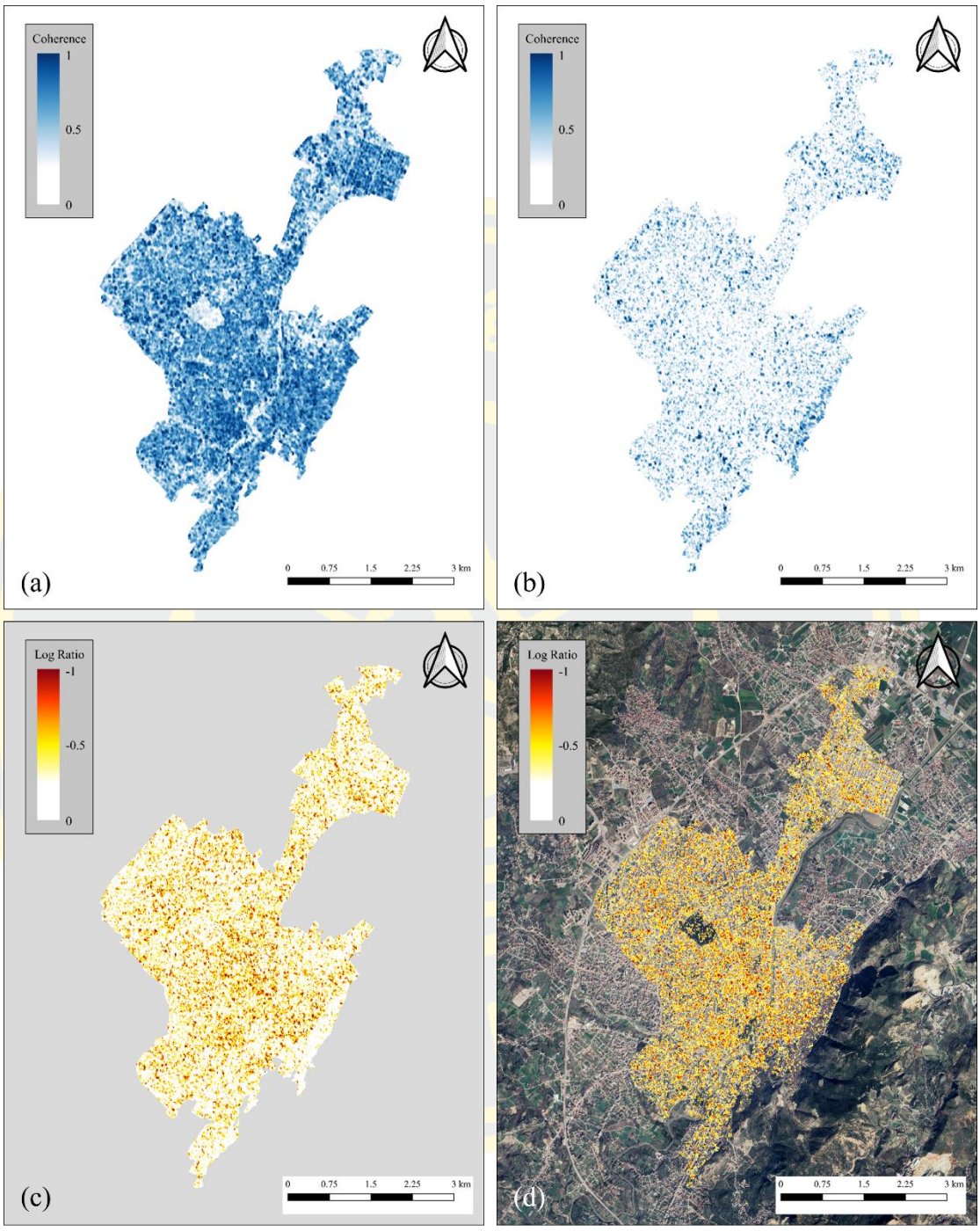

Figure 16 The urban area of Antakya (a) average pre-event coherence (b) post event coherence (c) log ratio (d) log ratio with the Google Earth base map.

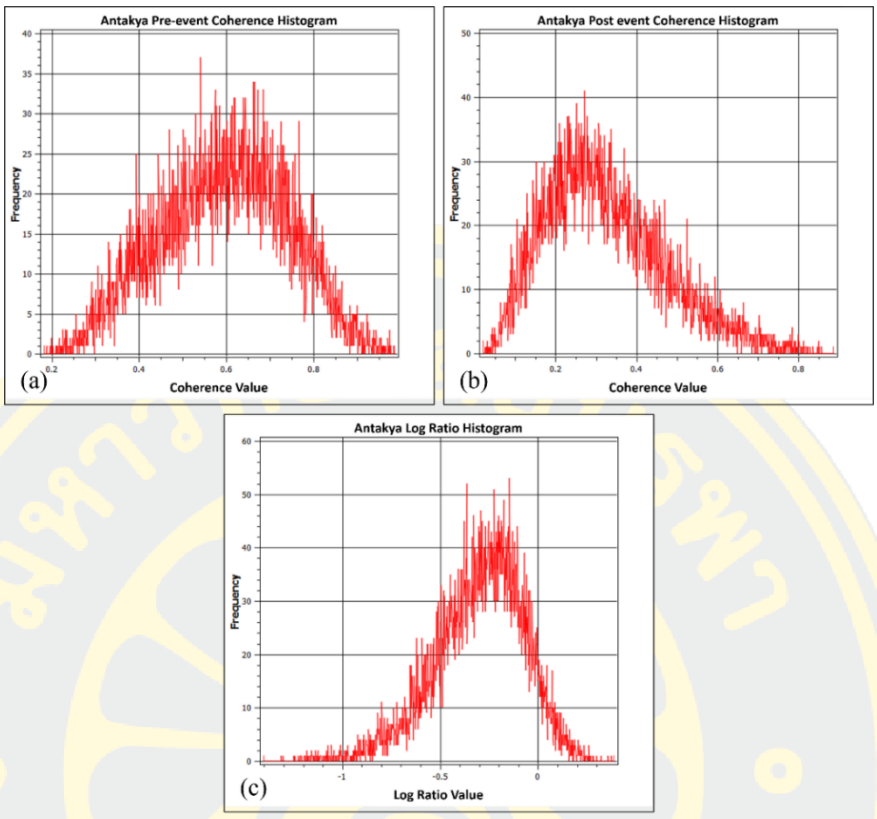

Figure 17 Histograms of the urban area of Antakya (a) average pre-event (b) post event (c) log ratio.

The coherence images of Antakya show that the coherence value reduced dramatically all over the area of interest after the earthquake. The histogram of the pre-event coherence shows the most frequent value around 0.6, then, the most frequent value reduced to 0.3 approximately. The log ratio images also show widespread changes all over the area of interest. However, the log ratio histogram shows that the most frequent change value is around -0.3 to -0.2 displayed in white colour in the log ratio image. In this study, we define the log ratio value that more than -0.3 as no change displayed in white, -0.5 to -0.3 as little change displayed in yellow, -0.7 to -0.5 as moderate change displayed in orange, and less than -0.7 as severe change displayed in red. We calculated the number of pixels by ranges of log ratio value and got the results that 44.58% of the area of interest were affected which includes little change at 26.50%, moderate change at 12.53%, and severe change at 5.55%.

Iskenderun

We created the area of interest for urban areas of Iskendrun as shown in Figure 18 and the results of the area of interest as shown in Figure 19 with histograms shown in Figure 20.

Figure 18 The area of interest for urban areas of Iskenderun.

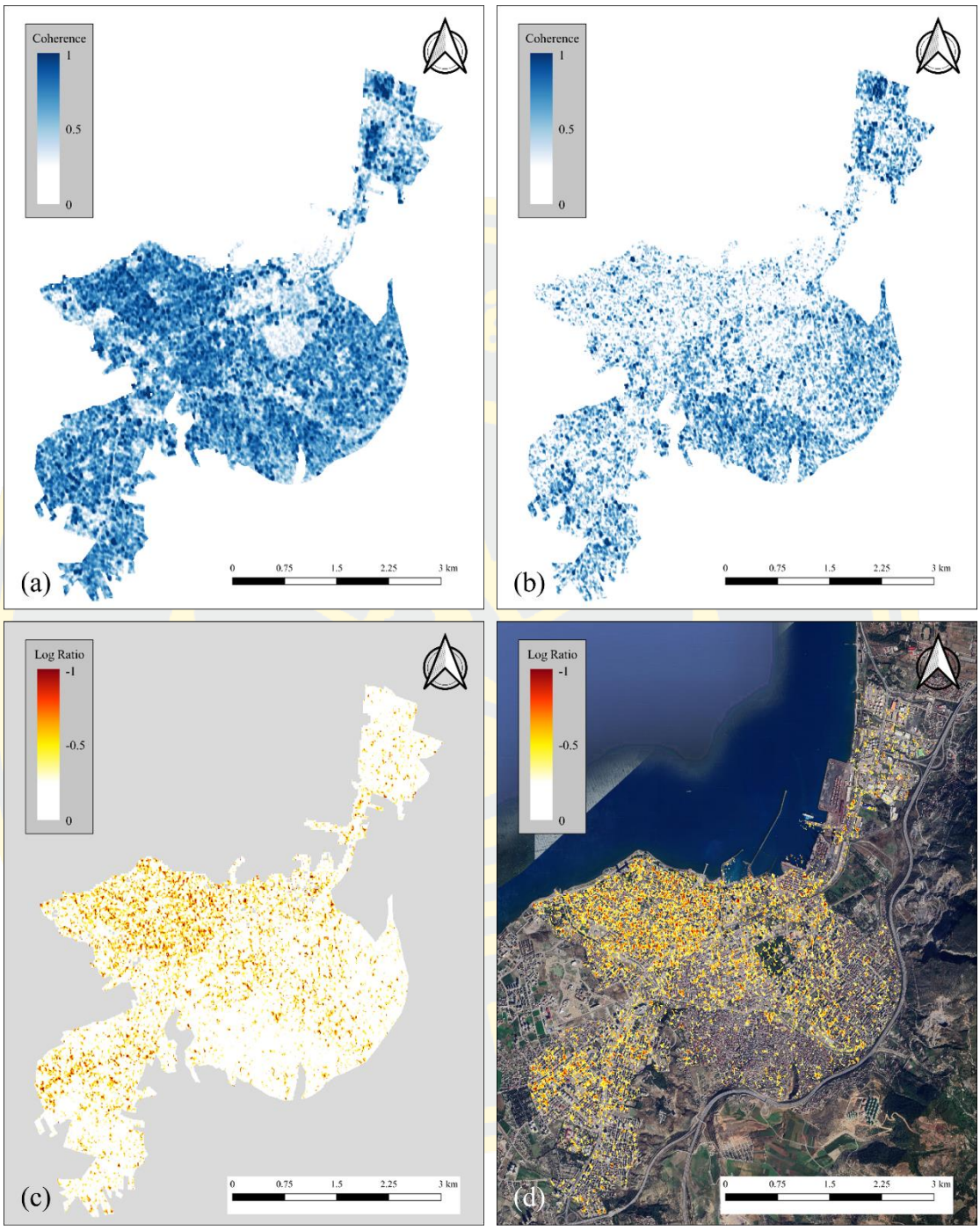

Figure 19 The urban area of Iskenderun (a) average pre-event coherence (b) post event coherence (c) log ratio (d) log ratio with the Google Earth base map.

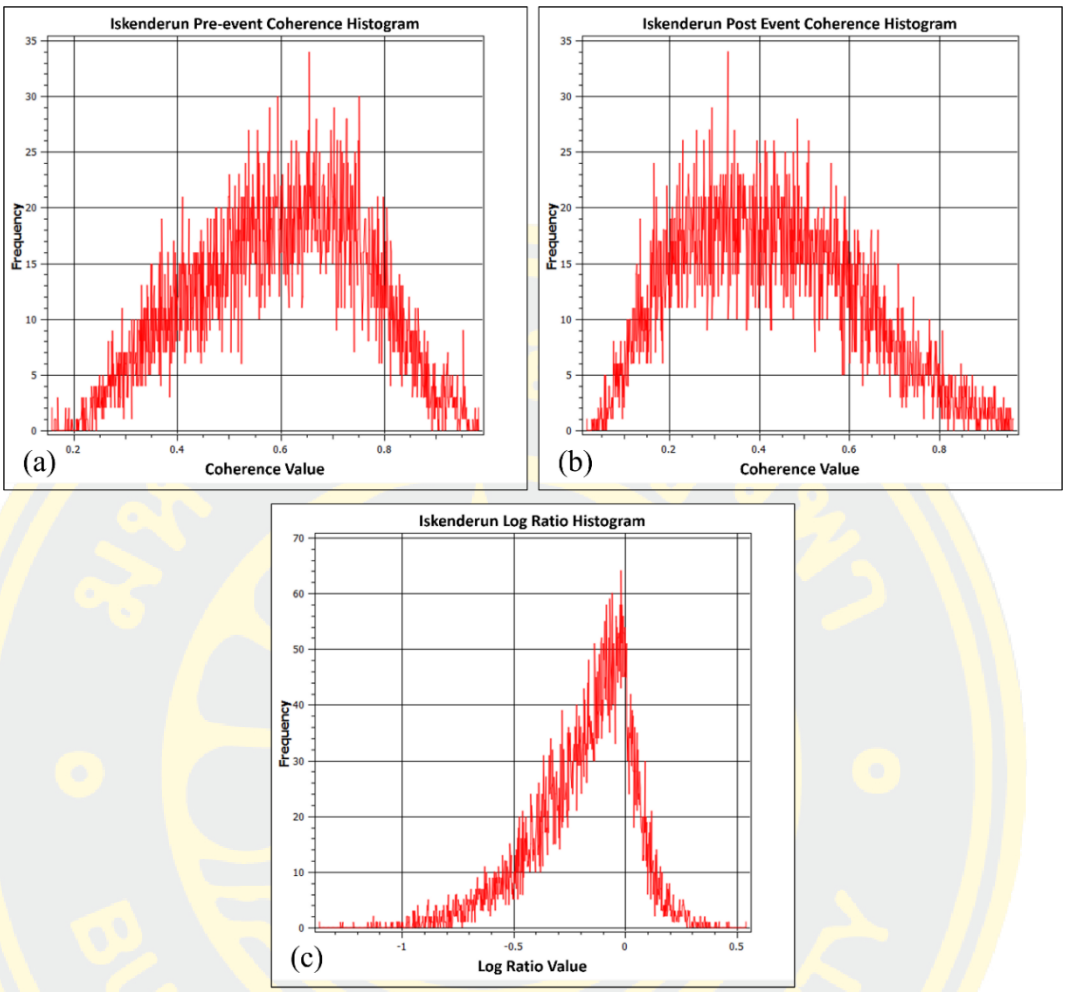

Figure 20 Histograms of the urban area of Iskenderun (a) average pre-event (b) post event (c) log ratio.

The coherence images of Iskenderun show that the coherence value dropped mostly in the north-western part of the city after the earthquake. The histogram of the pre-event coherence shows the most frequent value around 0.6–0.7, then, the most frequent value reduced to the range of 0.3–0.5. The log ratio images also show clusters of red, orange, and yellow colour mostly in the north-western part of the city. The log ratio histogram shows that the most frequent change value is between -0.2 to 0 which defined as no change. The data from the log ratio image were calculate, as a result, 24.09% of the area of interest were affected which includes little change at 15.68%, moderate change at 6.01%, and severe change at 2.40%.

Adana

We created the area of interest for urban areas of Adana as shown in Figure 21 and the results of the area of interest as shown in Figure 22 and 23 with histograms shown in Figure 24.

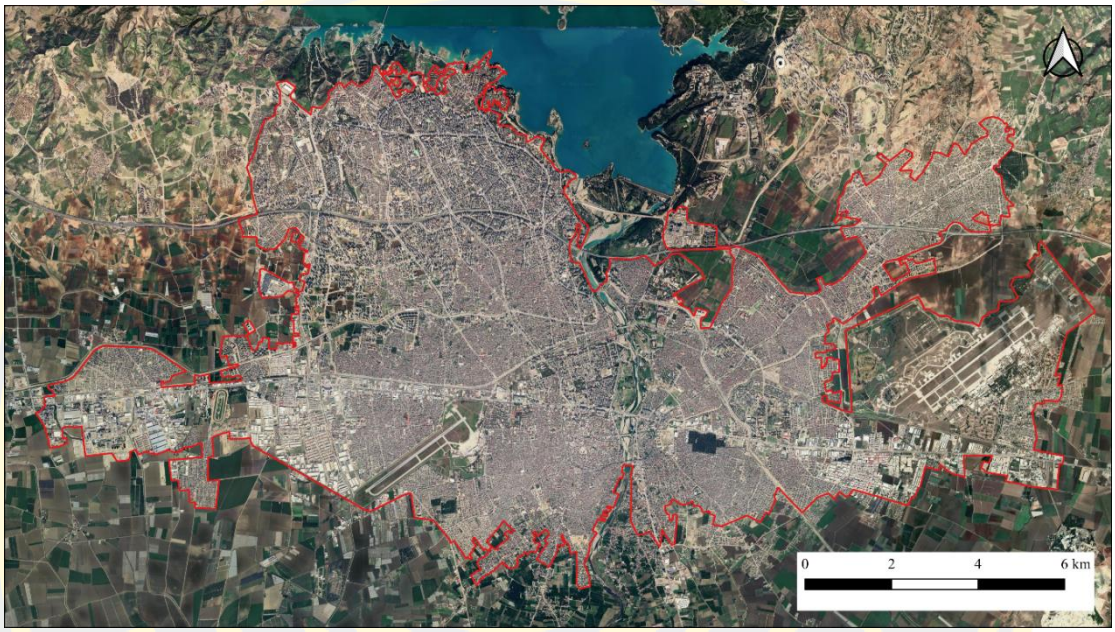

Figure 21 The area of interest for urban areas of Adana.

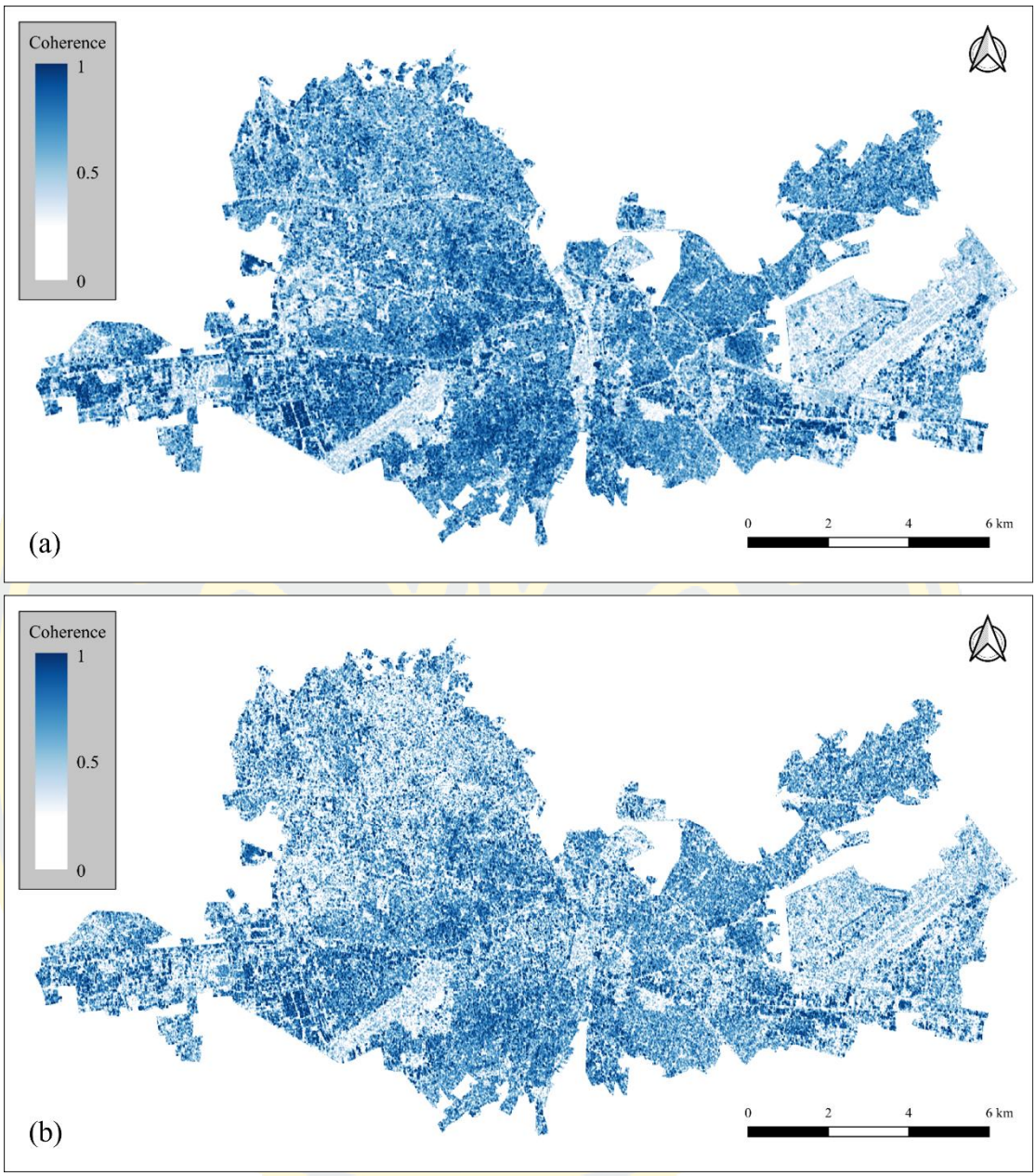

Figure 22 The urban area of Adana (a) average pre-event coherence (b) post event coherence.

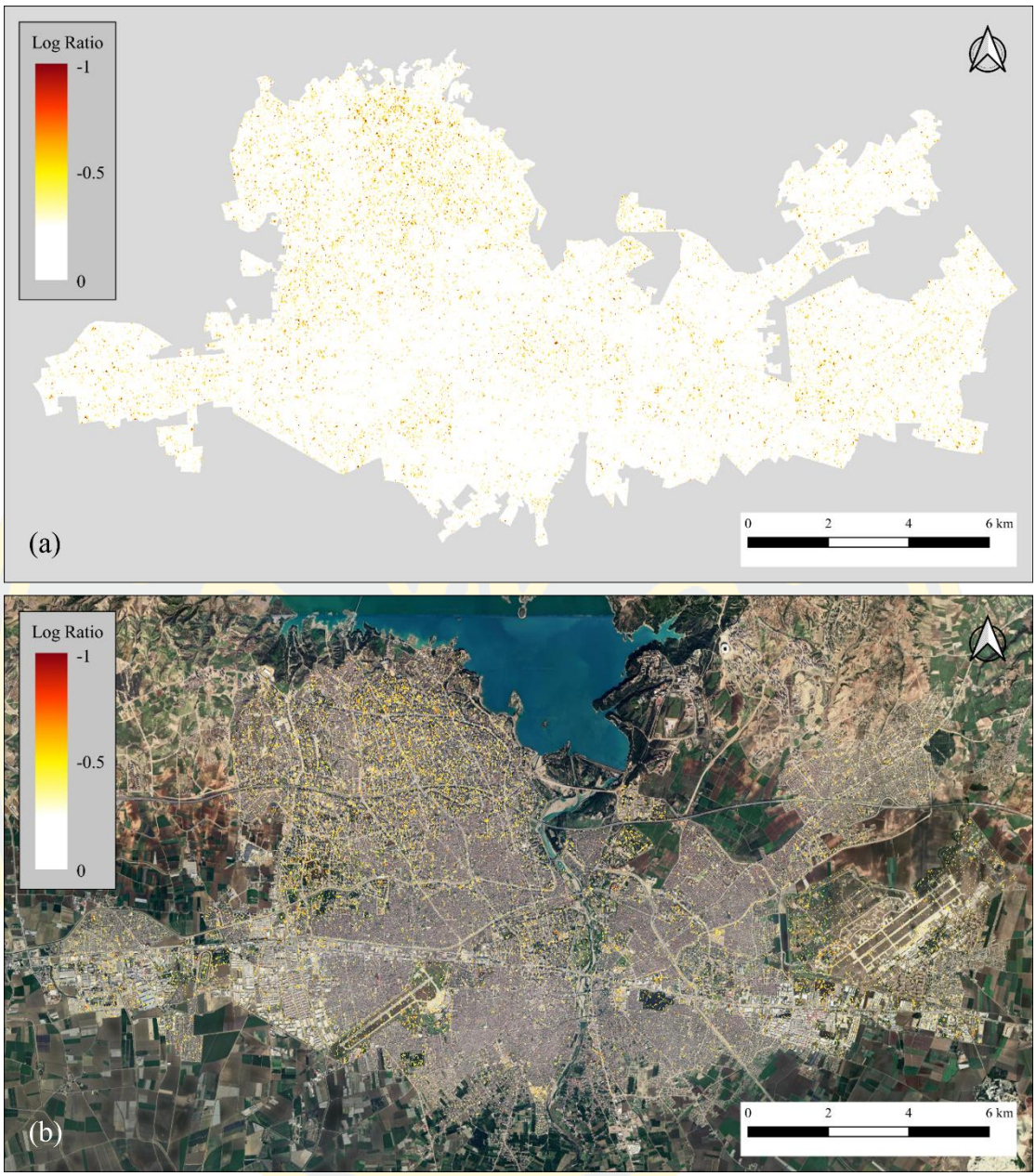

Figure 23 The urban area of Adana (a) log ratio (b) log ratio with the Google Earth base map.

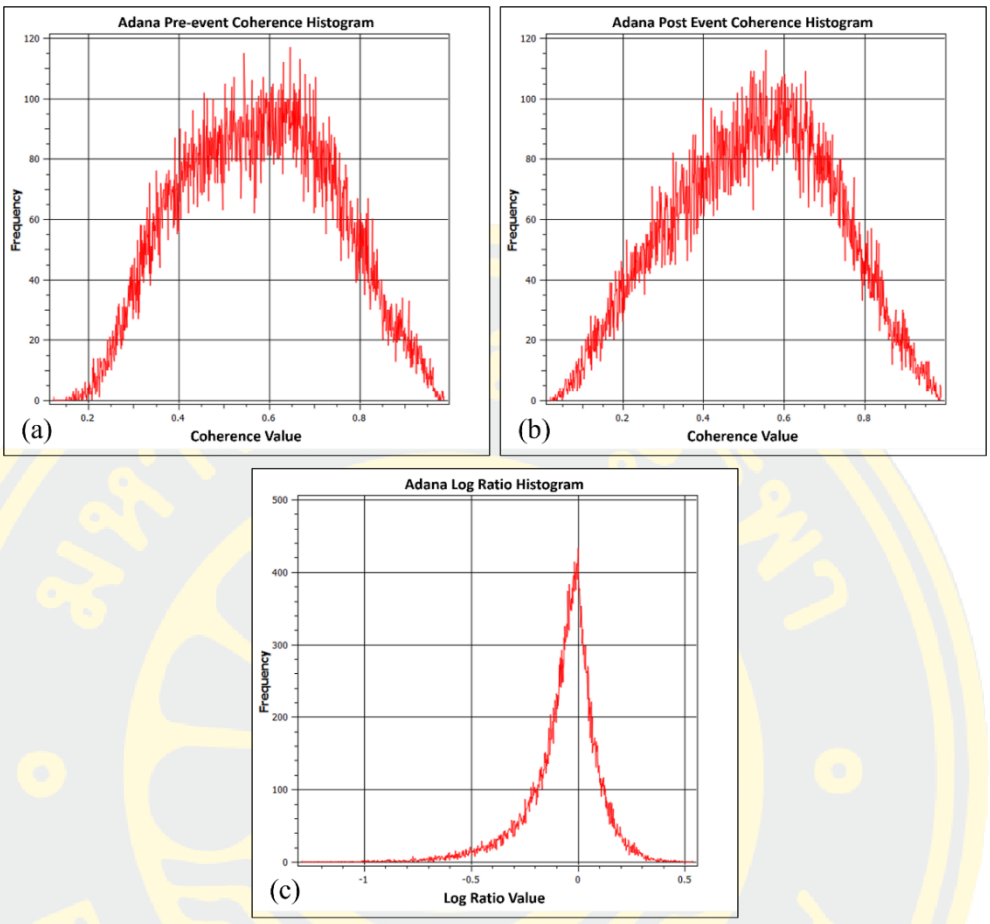

Figure 24 Histograms of the urban area of Adana (a) average pre-event (b) post event (c) log ratio.

The coherence images of Adana show not much change in coherence value after the earthquake. Most of the changes are in the northern part of the city. The coherence histograms of average pre-event image and post event image are not much different. The high frequency coherence value of average pre-event image is around 0.6–0.7 while the high frequency value of the post event coherence histogram is slightly fall to 0.5–0.6. We can see yellow colour wide spreads in the northern part of the city in log ratio image but not in a large cluster. The histogram of the log ratio image also indicates no change as we see the top of the graph is log ratio value of 0. The result calculated from log ratio value are, total affected area of interest at 7.79% including little change at 5.73%, moderate change at 1.58%, and severe change at 0.48%.

Ukraine

The results of the study area of Mariupol, Ukraine consist of 10 sets of an average pre-event coherence image, a post event coherence images, a log ratio image, and a log ratio with Google Earth overlay image which post event coherence images and log ratio images of these sets are the results from 20 February to 20 June 2022.

We created the area of interest for urban areas of Mariupol as shown in Figure 25 and the results of the area of interest as shown in Figure 26–35 with histograms shown in Figure 36 and 37.

Figure 25 The area of interest for urban areas of Mariupol.

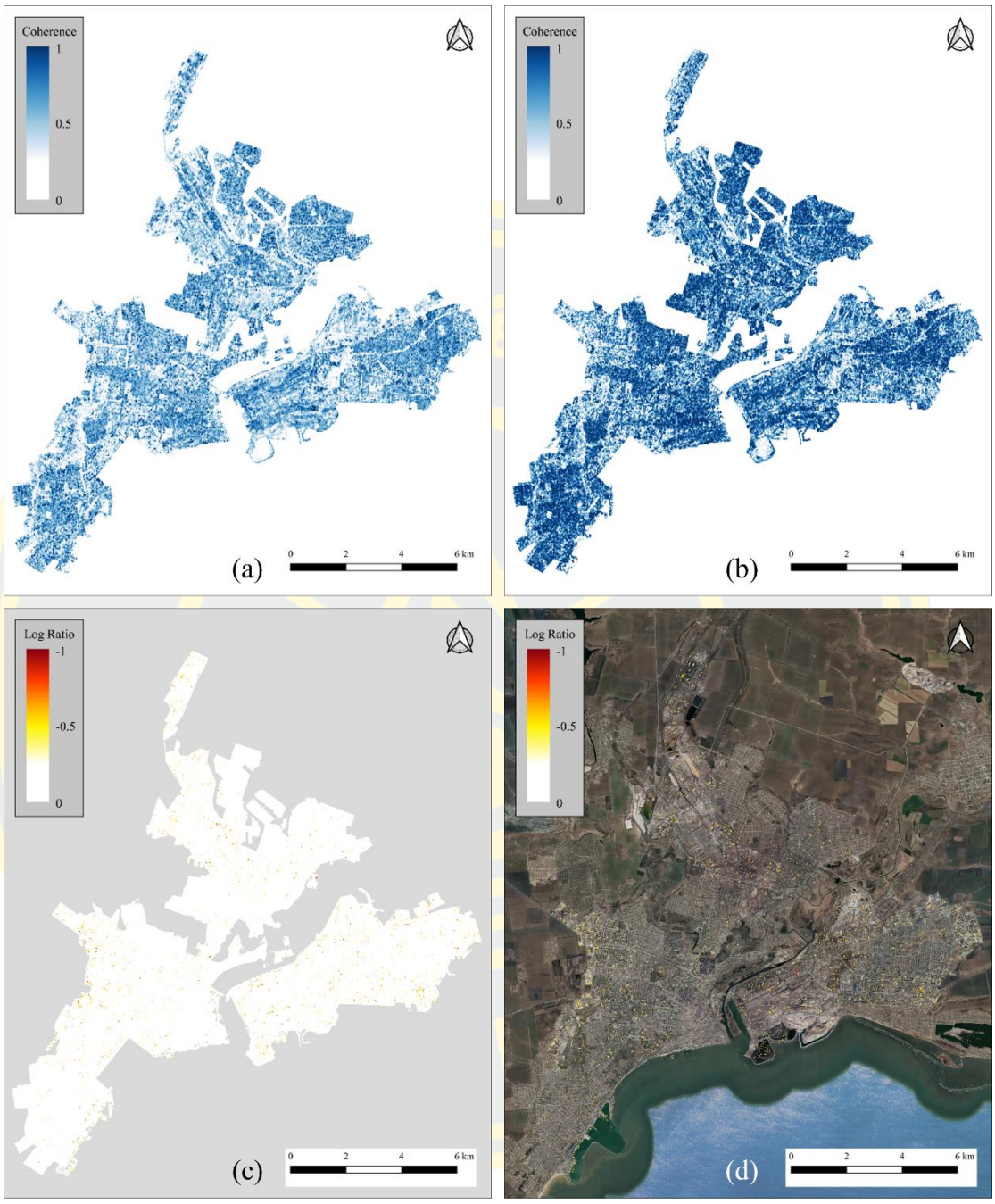

Figure 26 The urban area of Mariupol (a) average pre-event coherence (b) 20 February and 4 March 2022 coherence (c) log ratio (d) log ratio with the Google Earth base map.

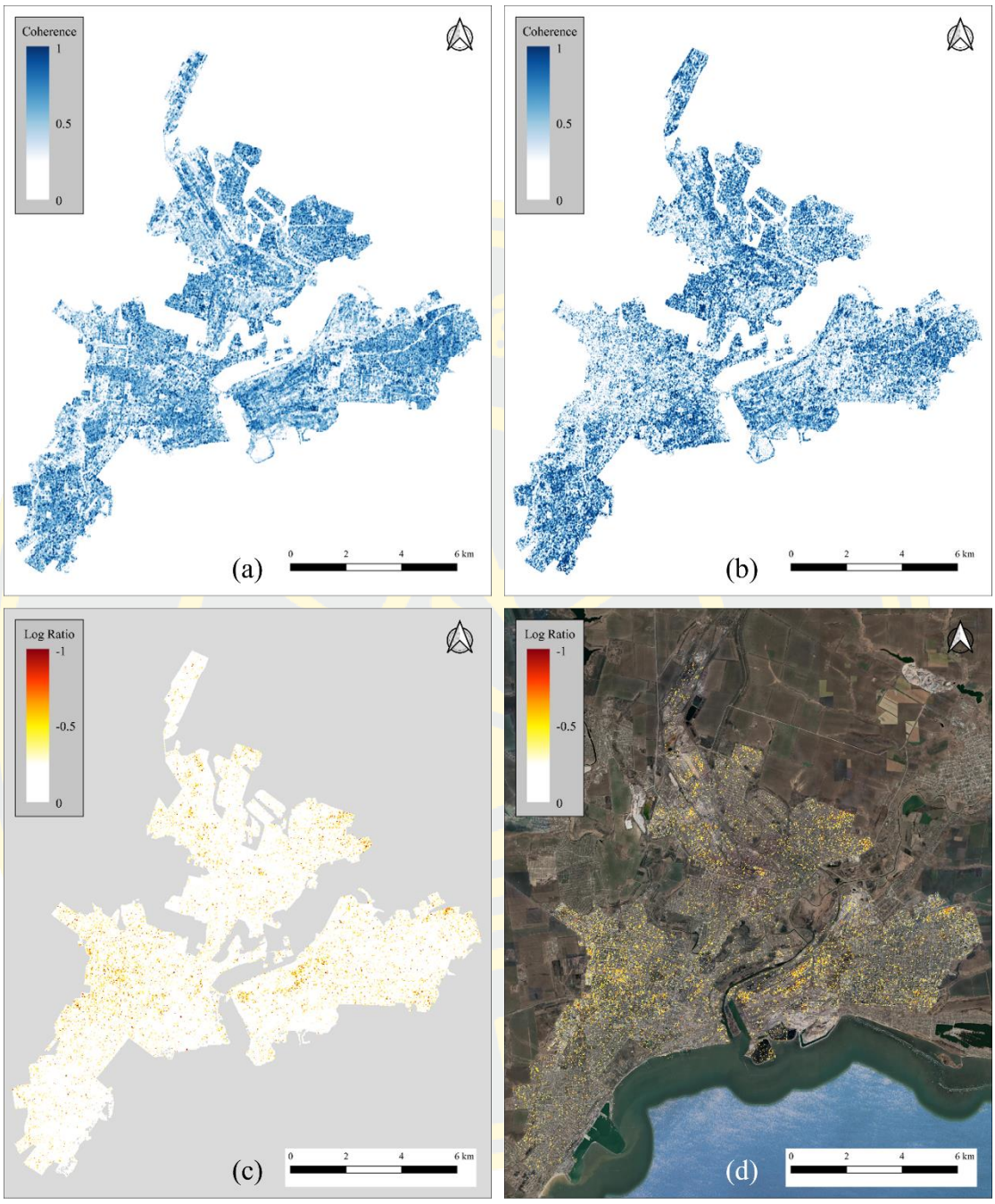

Figure 27 The urban area of Mariupol (a) average pre-event coherence (b) 4 and 16 March 2022 coherence (c) log ratio (d) log ratio with the Google Earth base map.

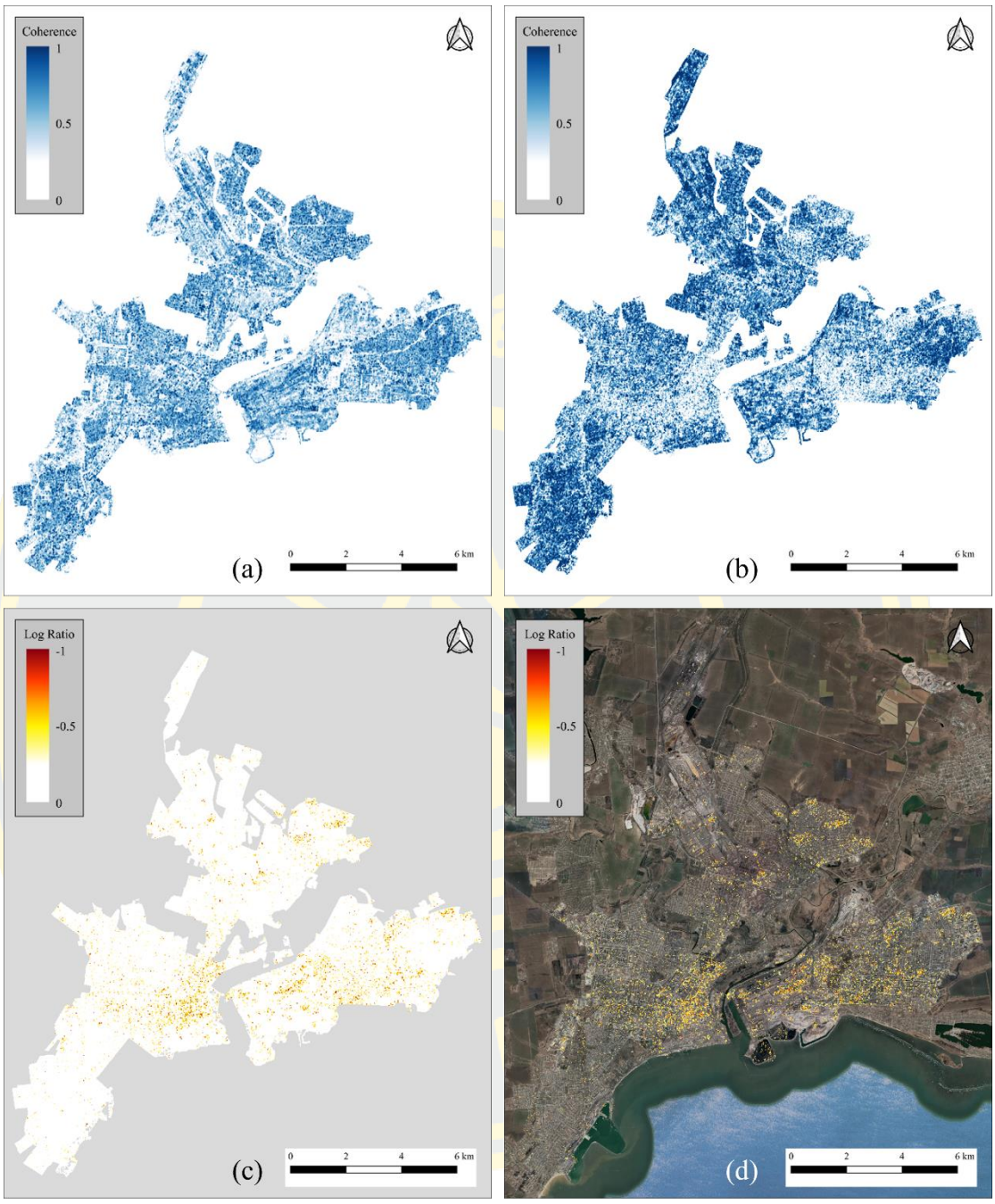

Figure 28 The urban area of Mariupol (a) average pre-event coherence (b) 16 and 28 March 2022 coherence (c) log ratio (d) log ratio with the Google Earth base map.

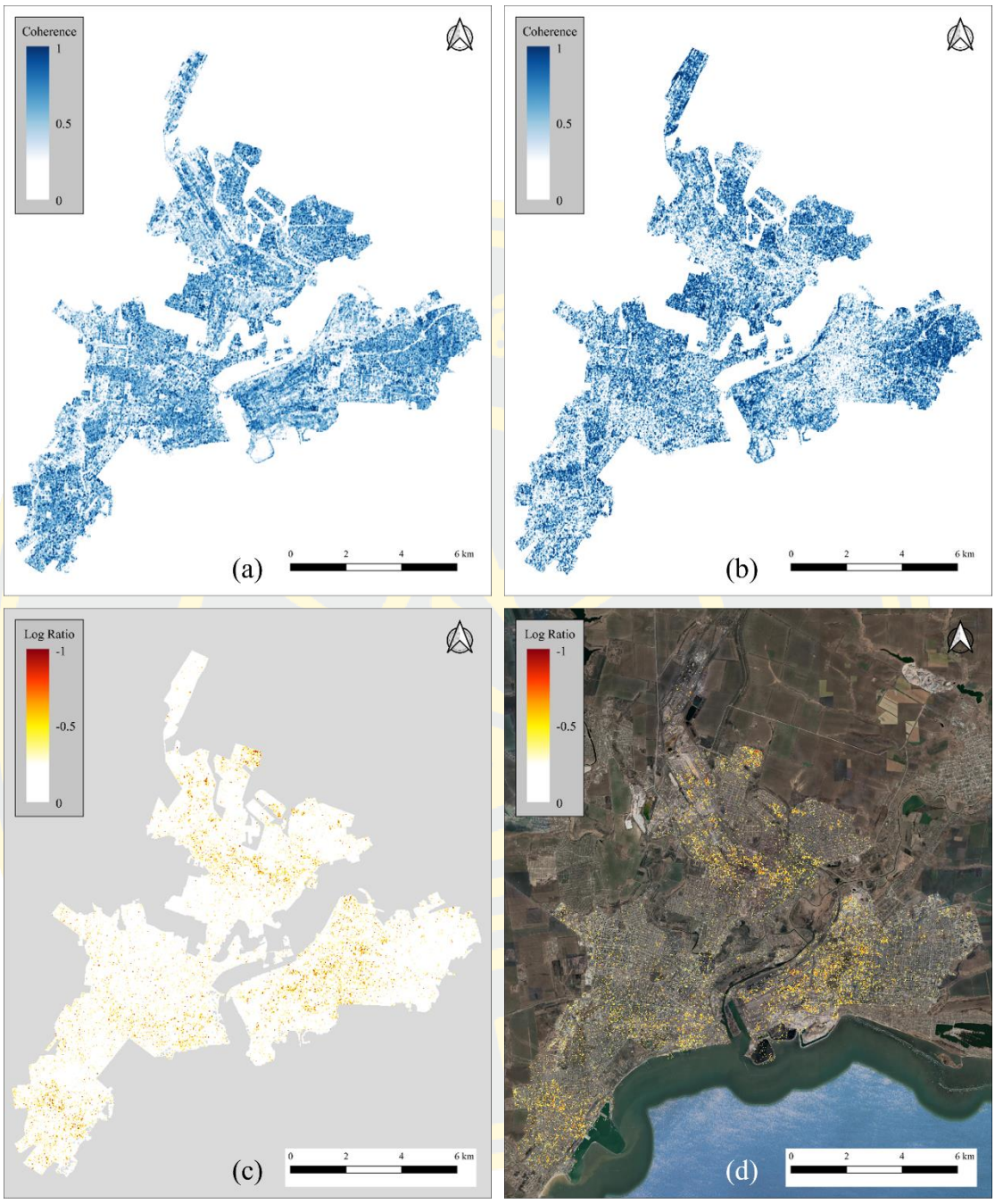

Figure 29 The urban area of Mariupol (a) average pre-event coherence (b) 28 March and 9 April 2022 coherence (c) log ratio (d) log ratio with the Google Earth base map.

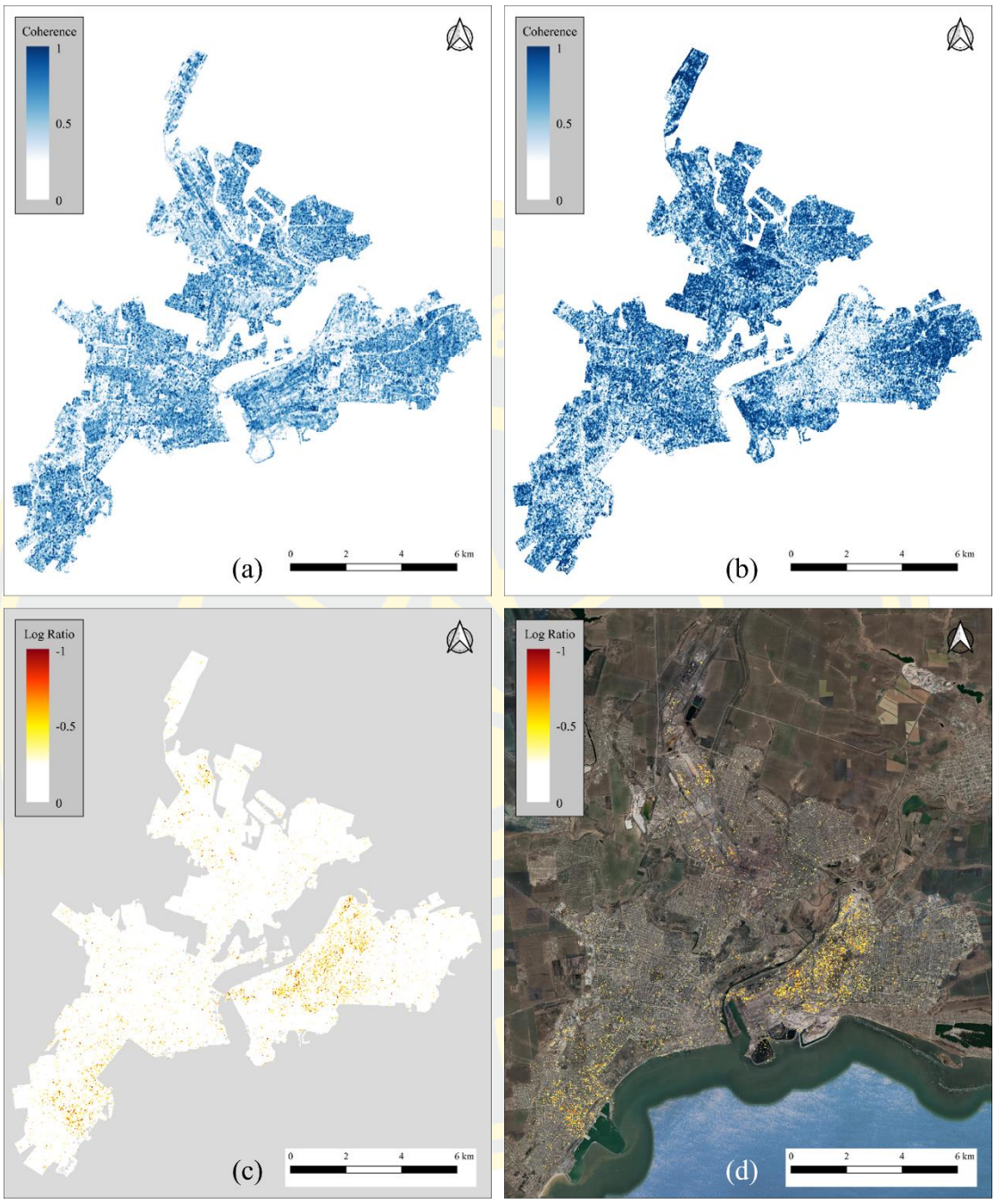

Figure 30 The urban area of Mariupol (a) average pre-event coherence (b) 9 and 21 April 2022 coherence (c) log ratio (d) log ratio with the Google Earth base map.

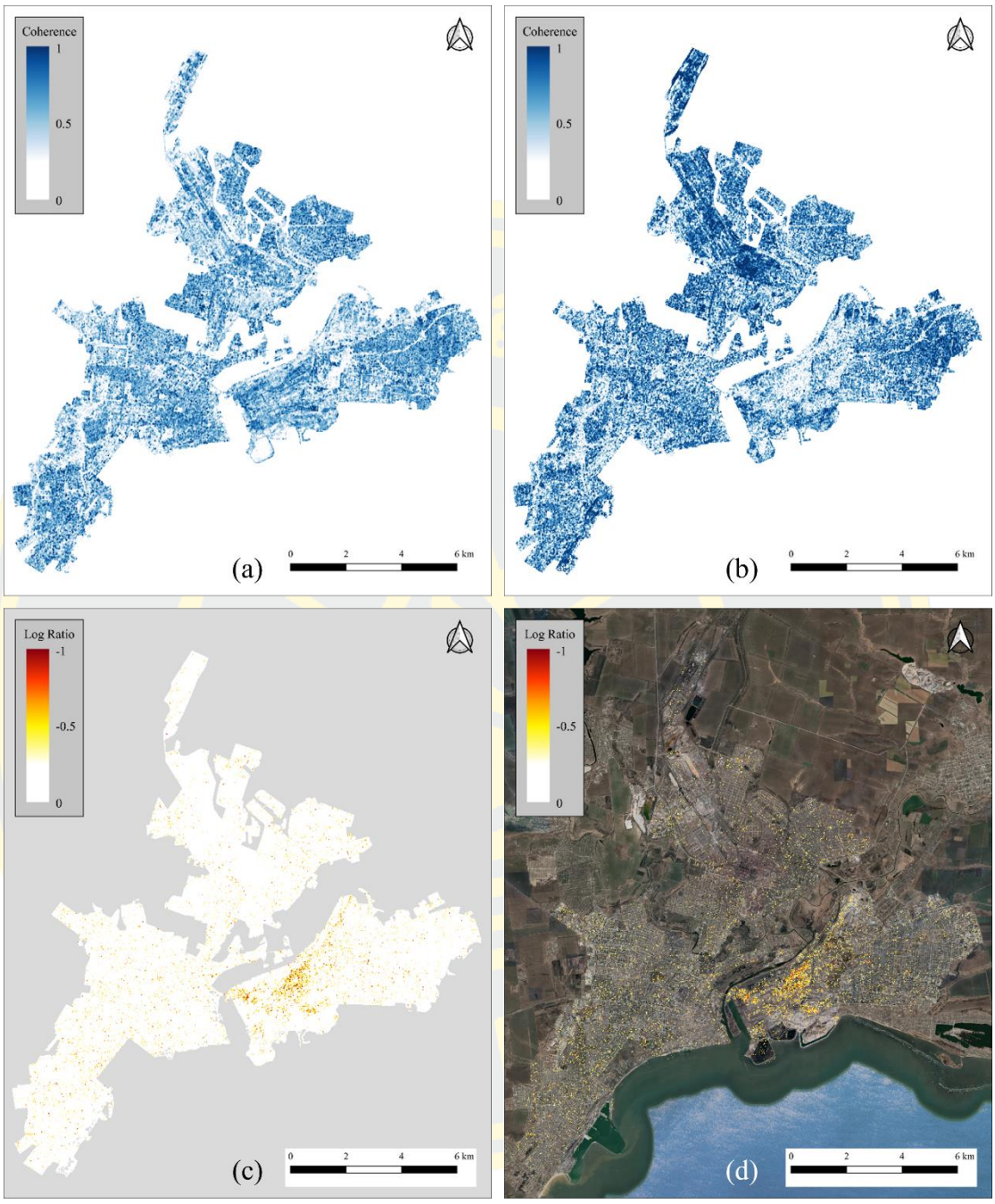

Figure 31 The urban area of Mariupol (a) average pre-event coherence (b) 21 April and 3 May 2022 coherence (c) log ratio (d) log ratio with the Google Earth base map.

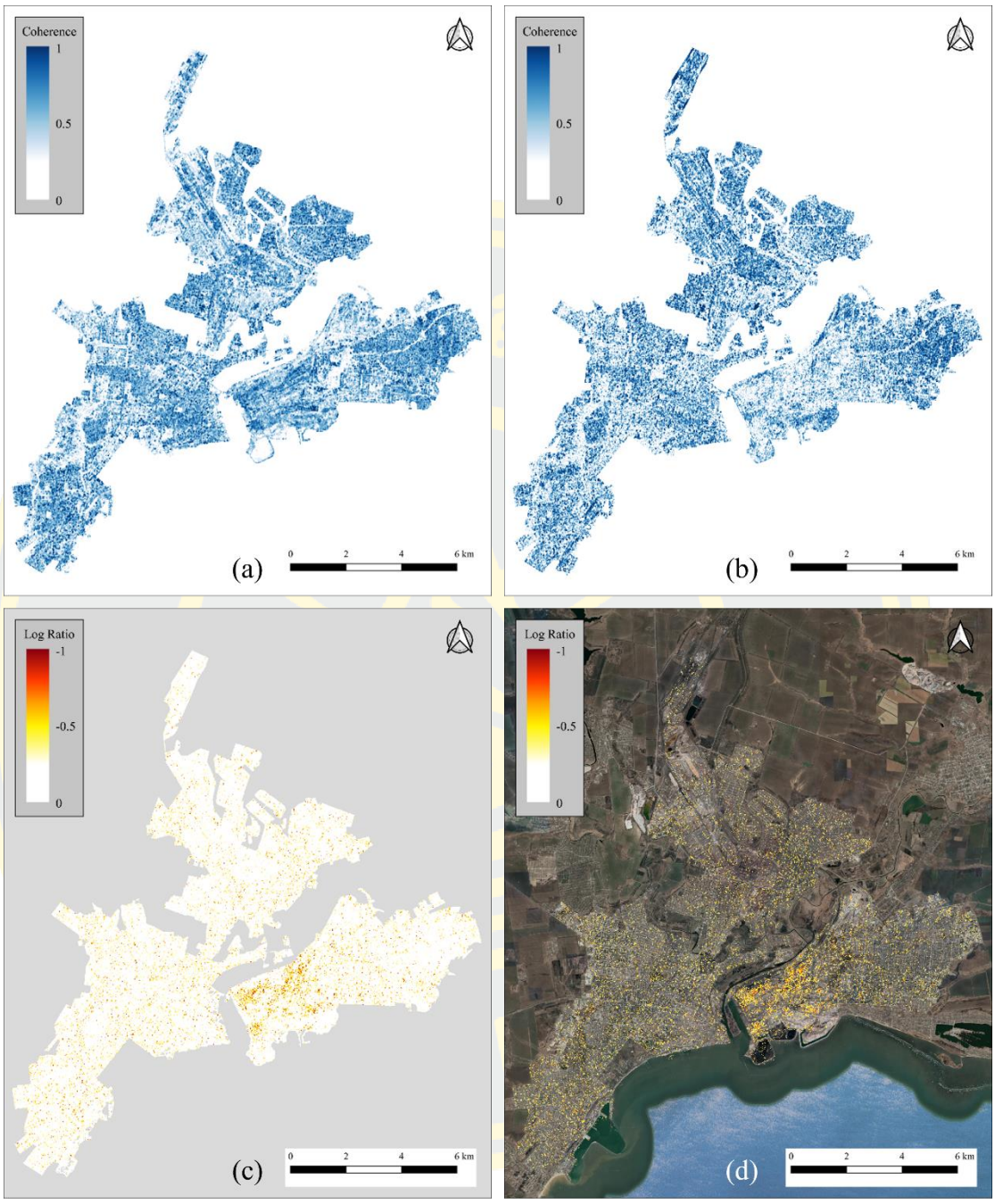

Figure 32 The urban area of Mariupol (a) average pre-event coherence (b) 3 and 15 May 2022 coherence (c) log ratio (d) log ratio with the Google Earth base map.

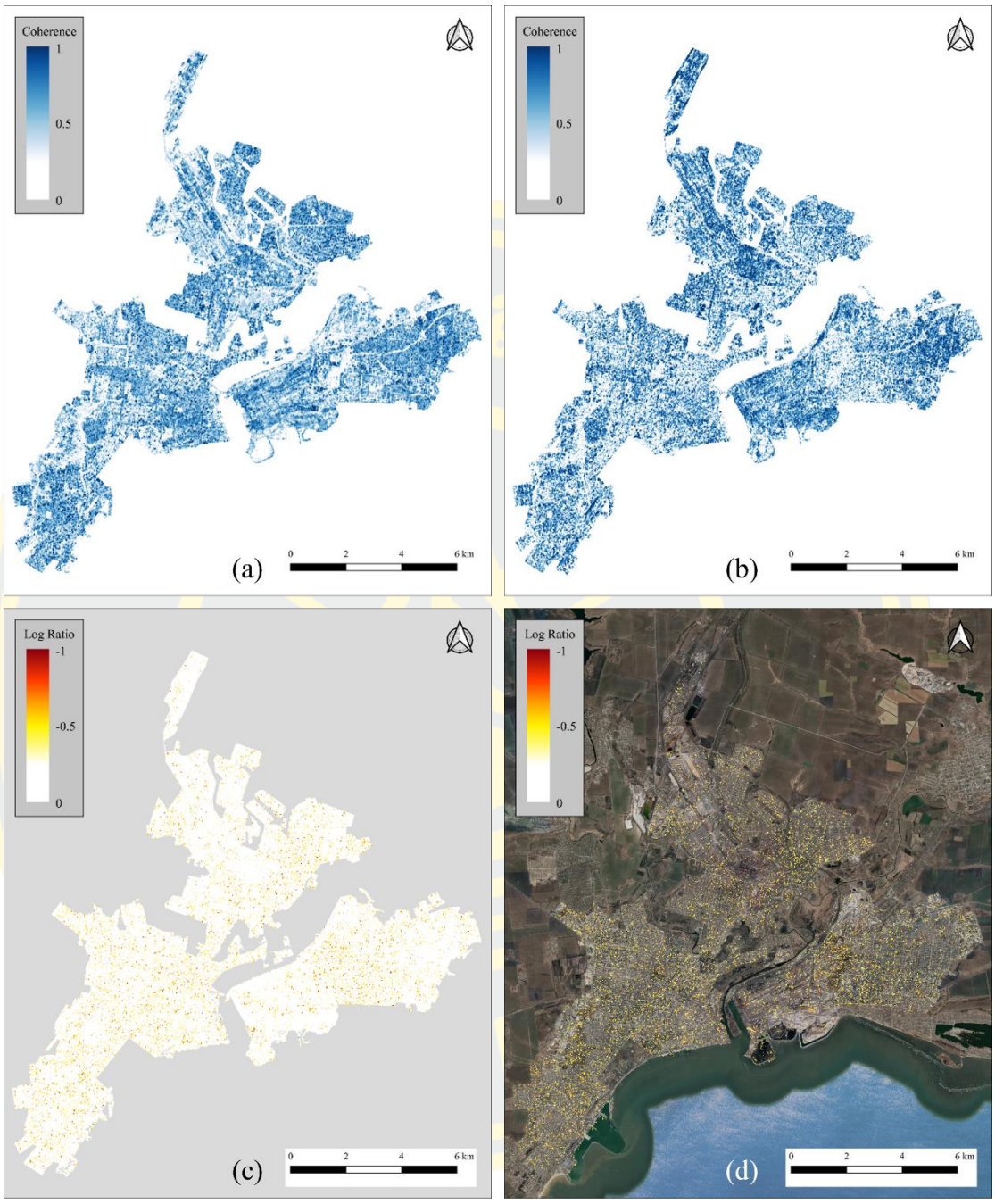

Figure 33 The urban area of Mariupol (a) average pre-event coherence (b) 15 and 27 May 2022 coherence (c) log ratio (d) log ratio with the Google Earth base map.

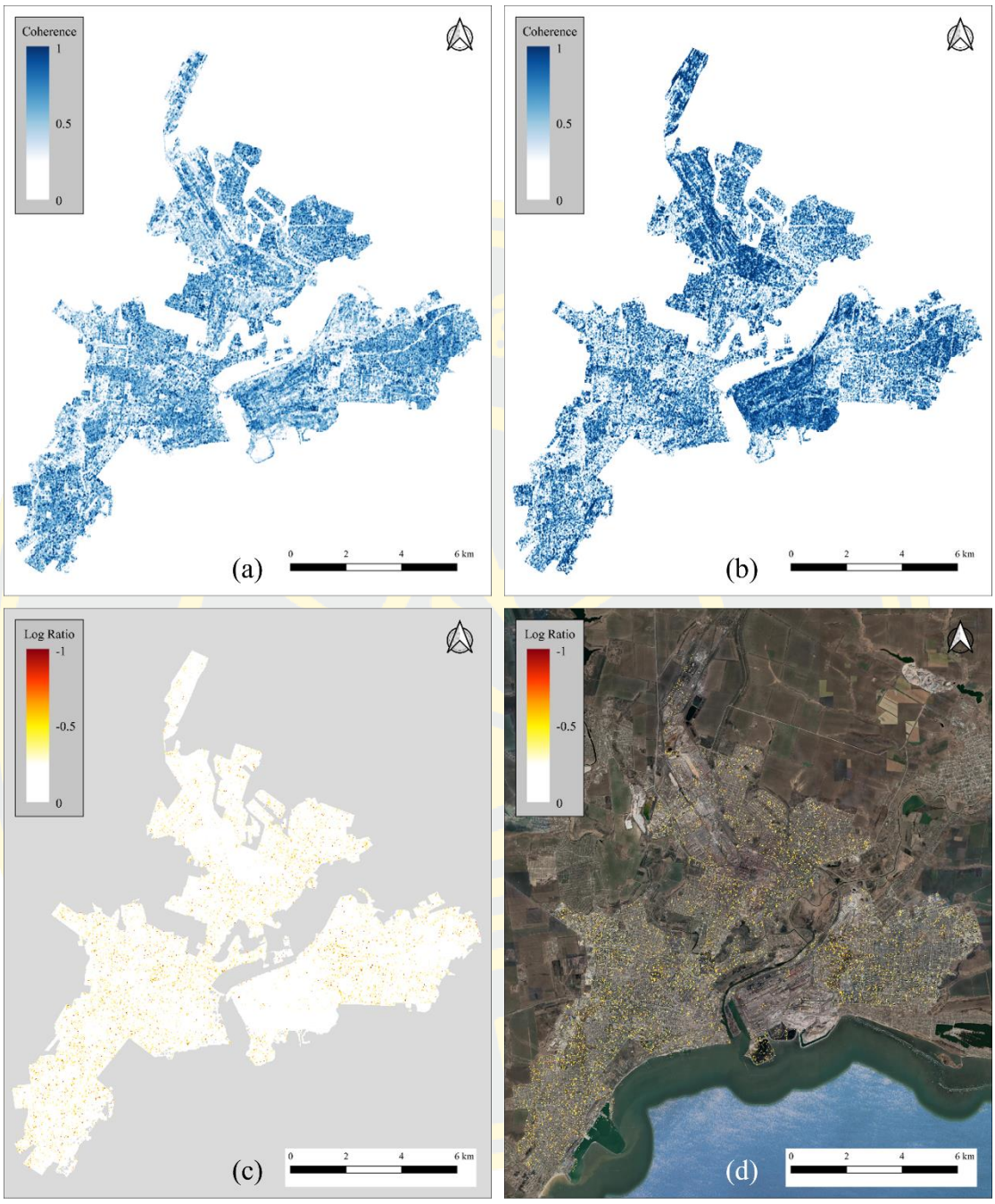

Figure 34 The urban area of Mariupol (a) average pre-event coherence (b) 27 May and 8 June 2022 coherence (c) log ratio (d) log ratio with the Google Earth base map.

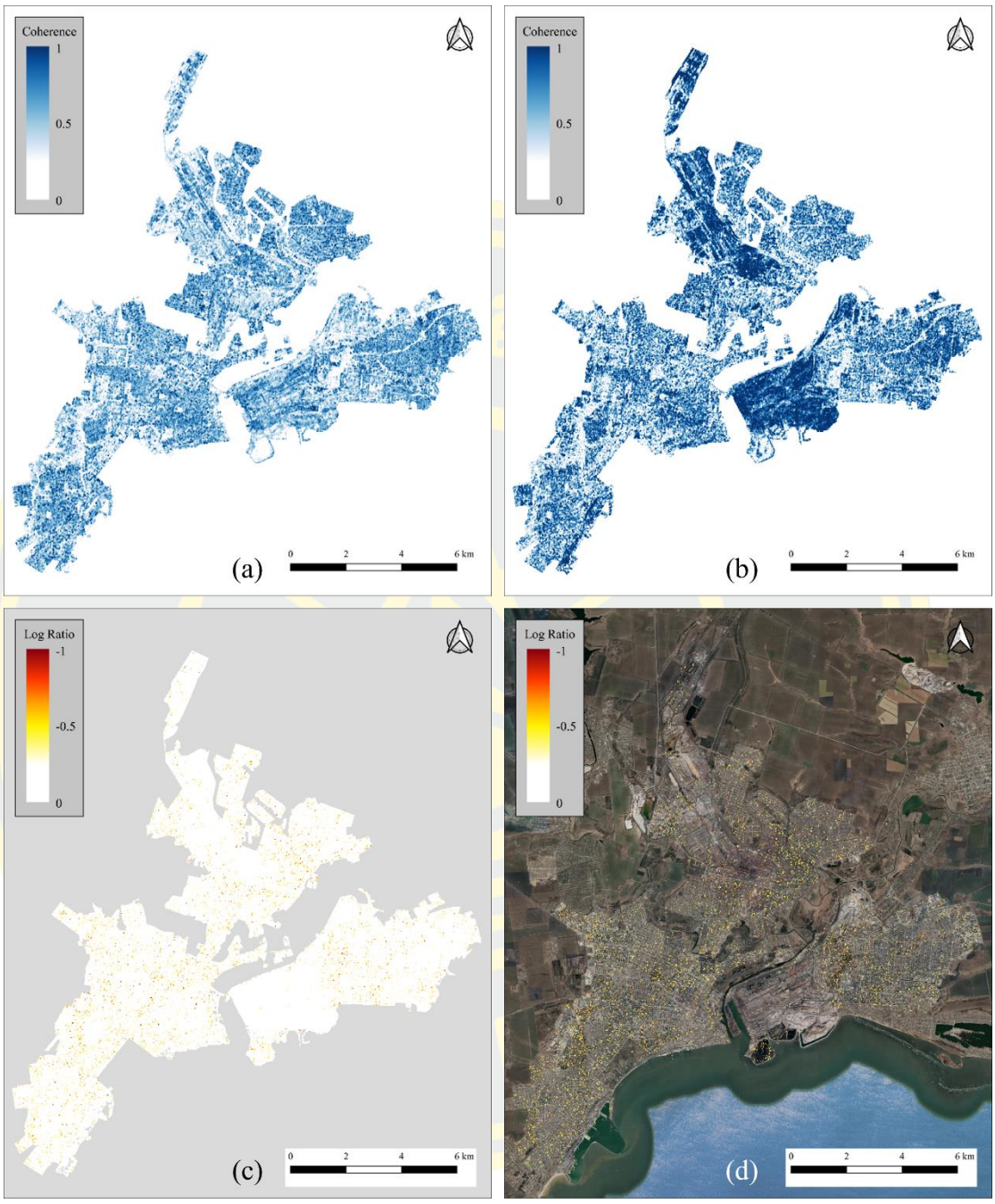

Figure 35 The urban area of Mariupol (a) average pre-event coherence (b) 8 and 20 June 2022 coherence (c) log ratio (d) log ratio with the Google Earth base map.

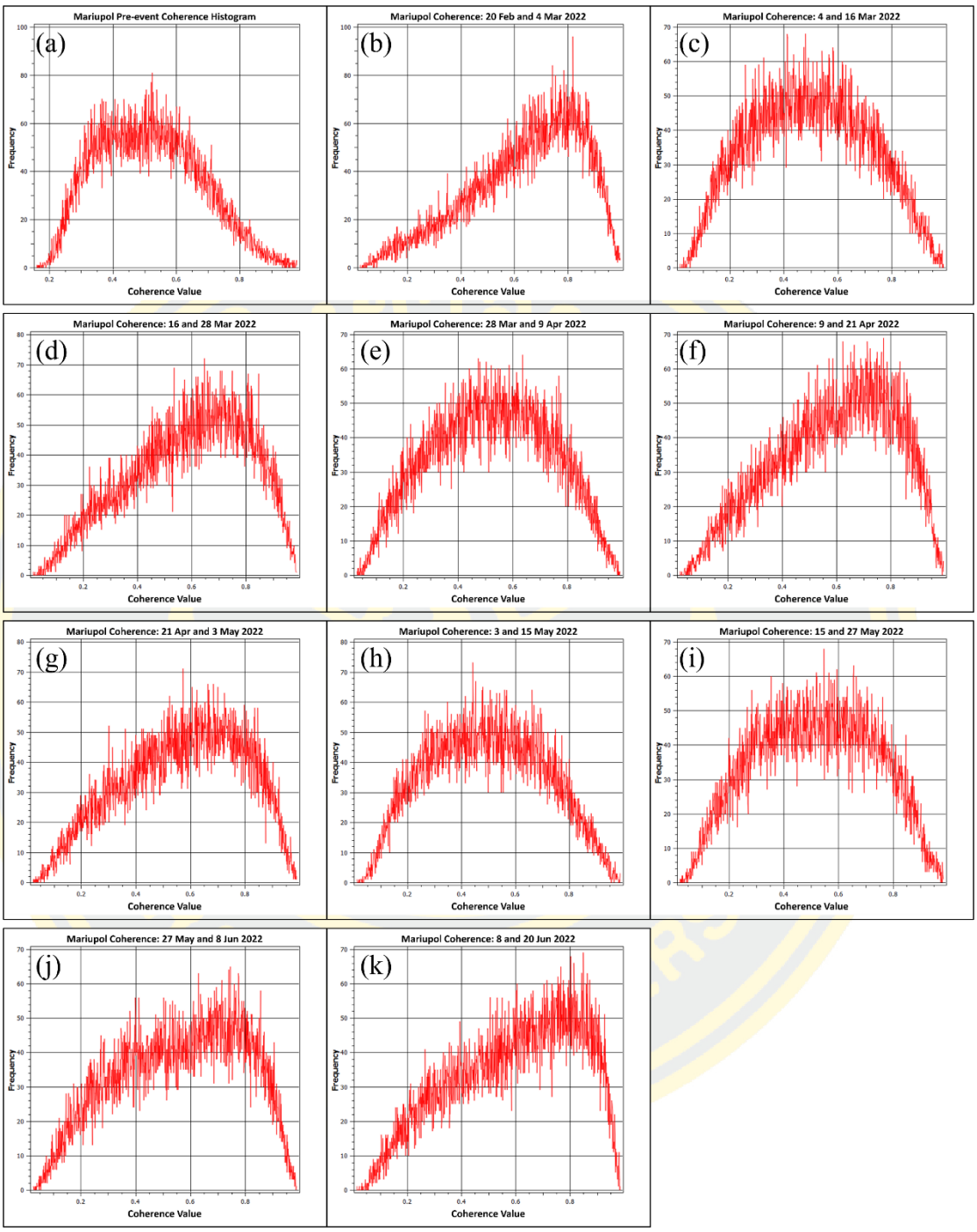

Figure 36 Histograms of the urban area of Mariupol (a) average pre-event (b–k) post event.

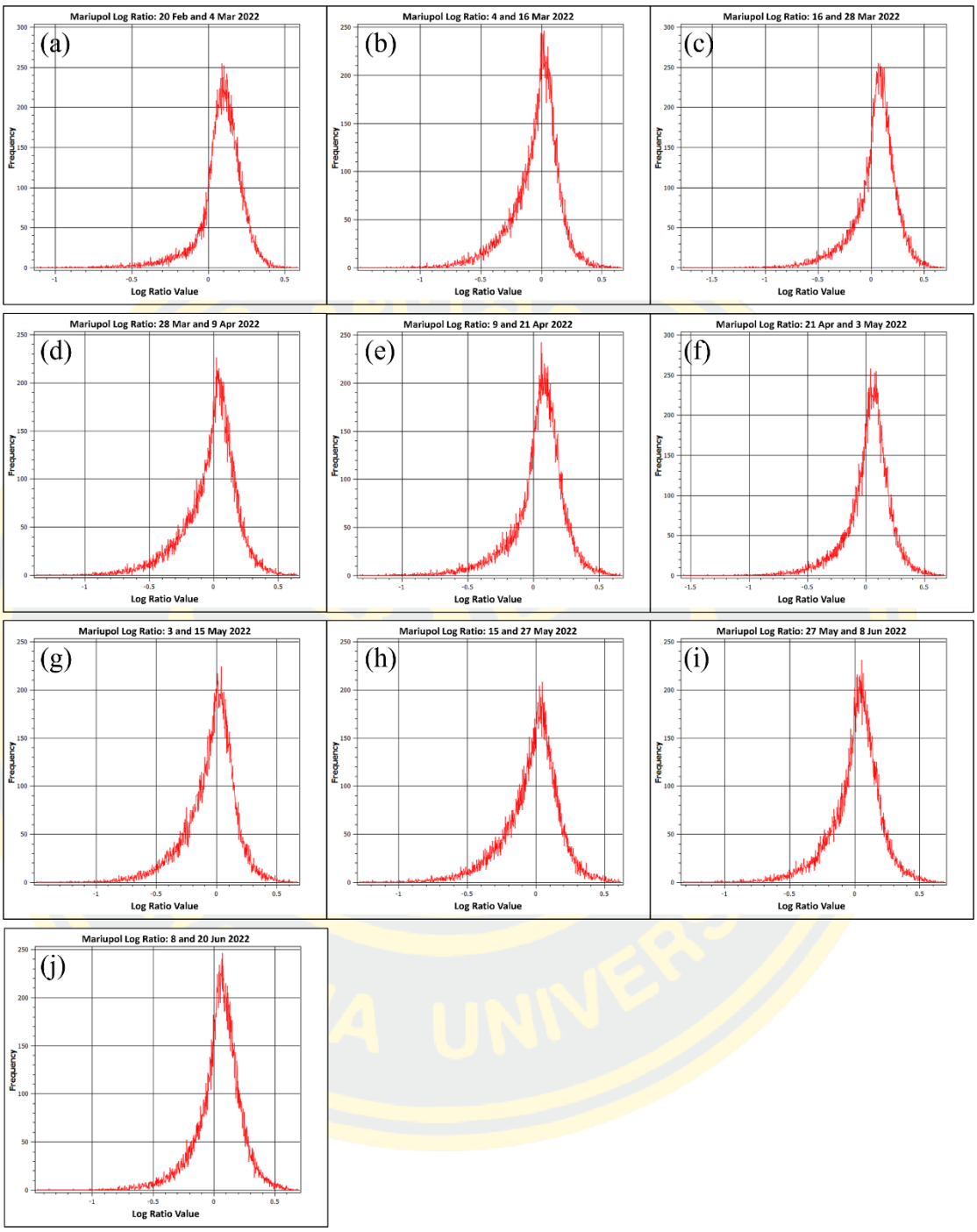

Figure 37 (a–j) Histograms of log ratio of the urban area of Mariupol.

For the study area of Mariupol, we can see from the coherence images that there was no change in the first two weeks of the invasion as the coherence histogram of this period shows the most frequent coherence value at 0.8, higher than the average

pre-event coherence image. The results of 4 and 16 March show changes as clusters, mostly in the western part of the city, some on the eastern edge of the area of interest, and nearby the area of Azovstal industrial site. From middle March to early April, the changes appeared mostly in the middle of the city. Then, from early April to middle May, the log ratio images show that there were significant changes in the area of Azovstal industrial site which located in the middle part of the city on the coast of the sea. After late May, there was no large cluster of change in the city. It appeared to be small points of changes widespread across the city, yet there was high coherence value in the area of Azovstal industrial site more than other parts of the city.

The coherence histograms show the high frequency value at around 0.4 to 0.6 in many periods of time because the intense changes occurred in the city were not in a large area. However, we cannot see much different in the log ratio histograms. The most frequent value of every log ratio histogram is around 0 to 0.2 which indicates that most of the area is no change.

We calculated the log ratio value of each log ratio image and classified as severe change, moderate change, little change, and no change as shown in Table 6.

Table 6 Percentage of log ratio value of Mariupol by levels of changes.

Period	Severe change	Moderate change	Little change	No change
20 Feb and 4 Mar 2022	0.14%	0.46%	1.61%	97.79%
4 and 16 Mar 2022	0.76%	2.28%	7.01%	89.95%
16 and 28 Mar 2022	0.61%	1.61%	4.67%	93.11%
28 Mar and 9 Apr 2022	0.82%	2.27%	6.57%	90.34%
9 and 21 Apr 2022	0.49%	1.33%	3.97%	94.21%
21 Apr and 3 May 2022	0.46%	1.34%	4.24%	93.96%
3 and 15 May 2022	0.88%	2.51%	7.73%	88.88%
15 and 27 May 2022	0.66%	2.04%	6.74%	90.56%
27 May and 8 Jun 2022	0.43%	1.46%	4.99%	93.12%
8 and 20 June 2022	0.34%	1.11%	3.83%	94.72%

When we combined the log ratio data from 10 log ratio images to estimate changes from the beginning of the invasion until June 2022, we found that 44.88% of the area of interest were affected including little change at 26.76%, moderate change at 12.88%, and severe change at 5.24%.

Result Comparison

To compare our results, we used pre-event images and post event images from Google Earth in selected locations for each study area. The collapsed or severely damaged buildings that can obviously be seen in the Google Earth images also result in the log ratio images in red as shown as shown in Figure 38–41.

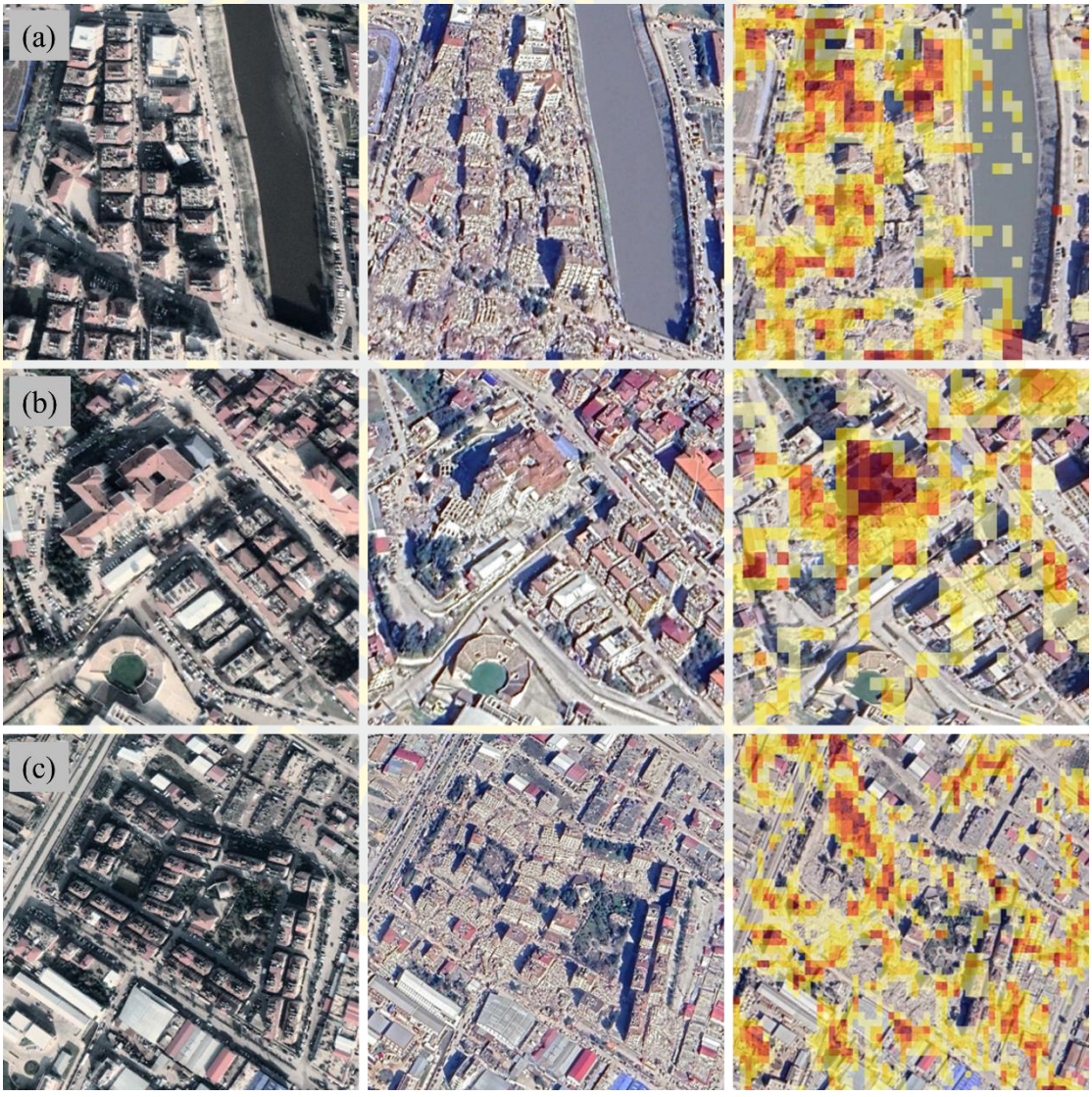

Figure 38 Comparison of the results of Antakya. The locations (a–c) were selected as representative areas for comparison. The columns from left to right indicate the Google Earth images of 22 December 2022, 9 February 2023, and 15 February 2023 with log ratio image overlay.

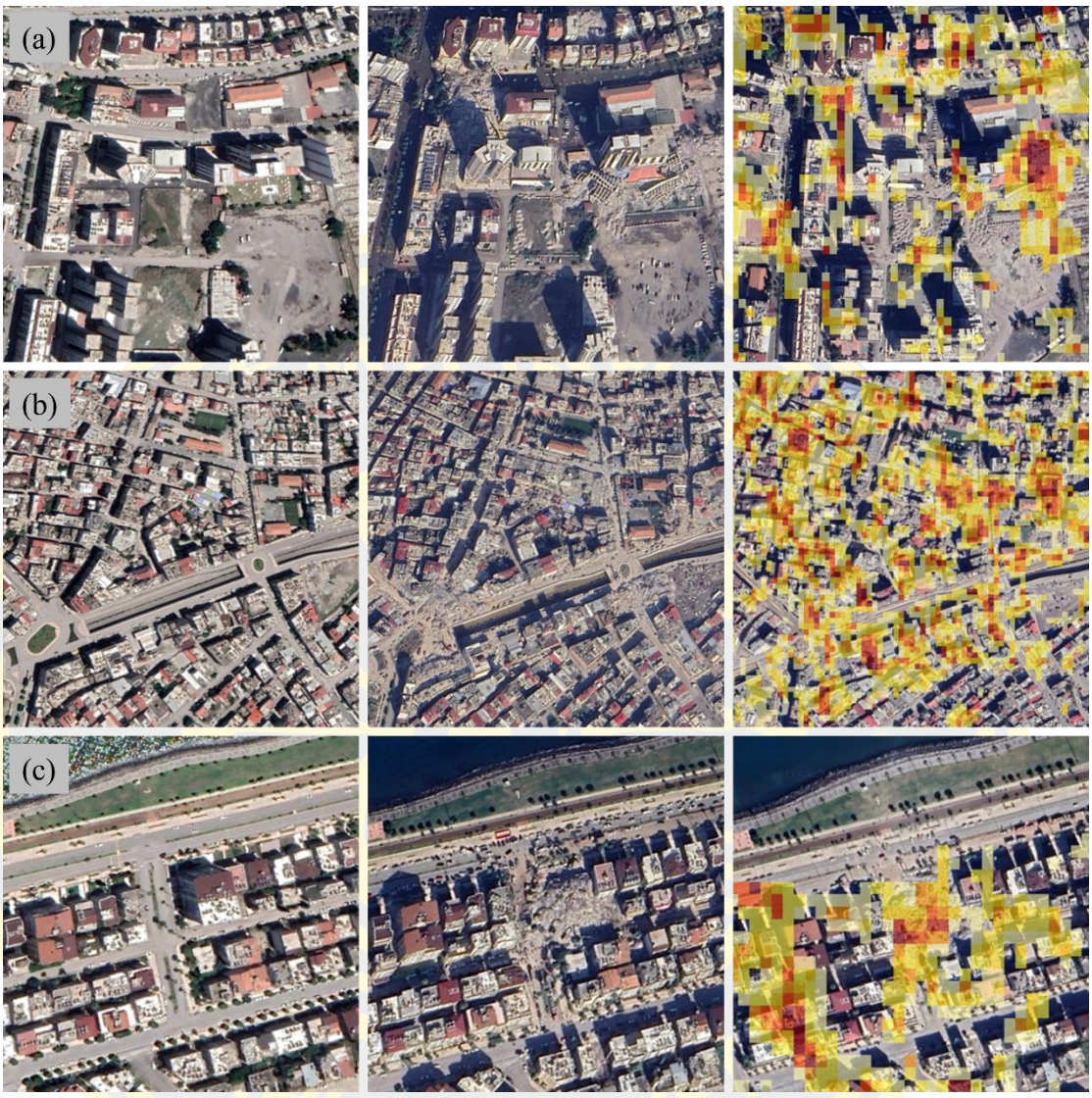

Figure 39 Comparison of the results of Iskenderun. The locations (a–c) were selected as representative areas for comparison. The columns from left to right indicate the Google Earth images of 26 December 2022, 9 February 2023, and 17 February 2023 with log ratio image overlay.

Figure 40 Comparison of the results of Adana. The locations (a–c) were selected as representative area for comparison. The columns from left to right indicate the Google Earth images of 17 October 2022, 9 February 2023, and 17 February 2023 with log ratio image overlay.

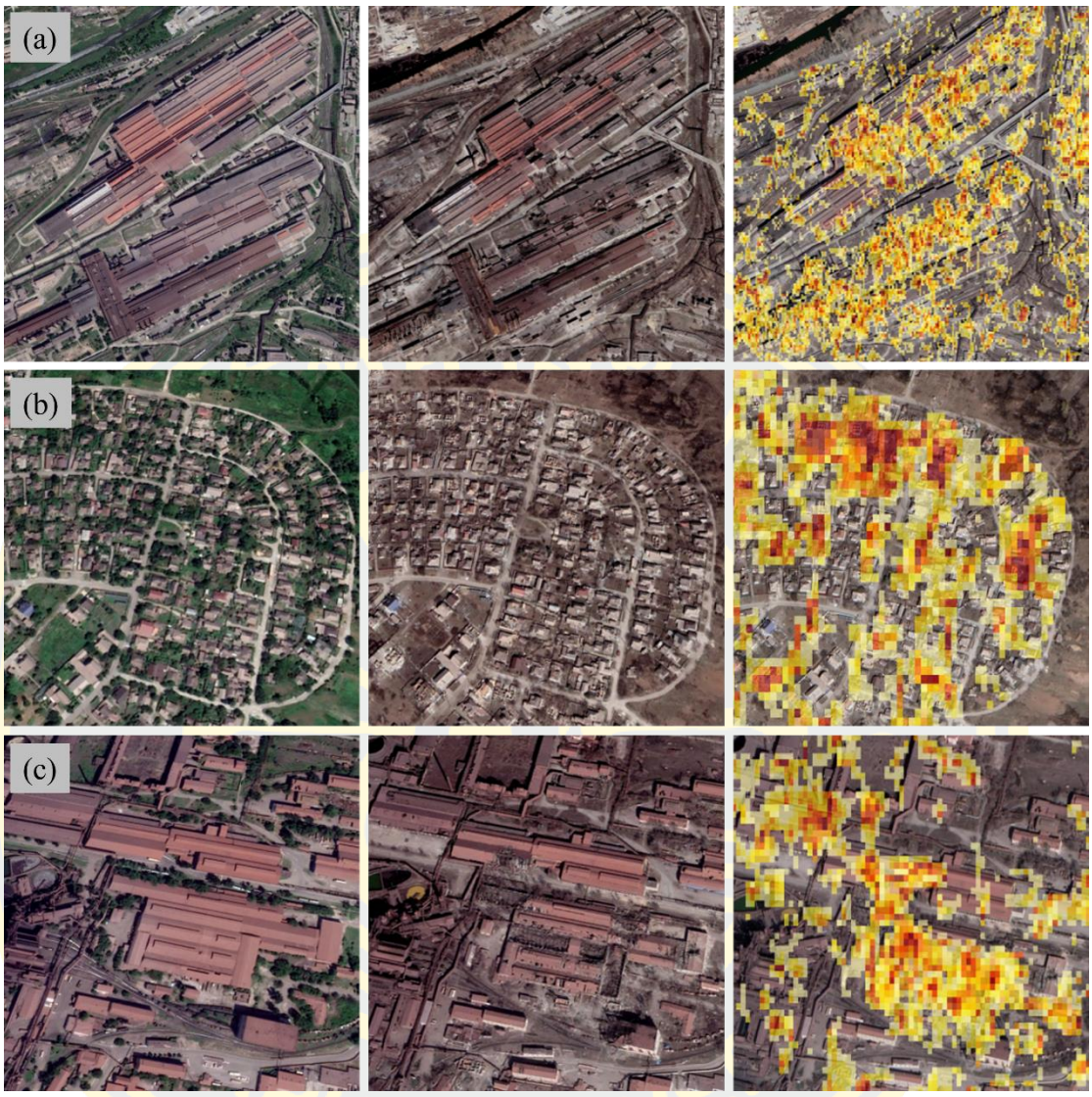

Figure 41 Comparison of the results of Mariupol. The locations (a–c) were selected as representative areas for comparison. The columns from left to right indicate the Google Earth images of 21 June 2021, 29 March 2022, and 29 March 2022 with log ratio image overlay.

CHAPTER 5
DISCUSSION AND CONCLUSION

This chapter is the final chapter which consists of 2 parts including a discussion and a conclusion of this study.

Discussion

This study presented the potential use of Sentinel-1 images with the coherence change detection technique for damage assessment in two situations of disasters including the earthquake in Turkey occurred in 2023 and the invasion of Russia in Ukraine began in 2022. In this study, we focused on the decreasing of coherence to monitor changes and destruction of the urban areas. The results in the experiments showed significant loss of coherence after the earthquake all over the area of Antakya. The urban areas of Antakya were the most affected by the earthquake compared to Iskenderun and Adana. According to Bogazici University researchers, Antakya experienced more severe ground motion than other cities (Şeşetyan, Stucchi, Castelli, & Gómez Capera, 2023). Antakya and Iskenderun are in Hatay province which reported to be the worst affected province (Gunasekera et al., 2023). The results showed that 45% of urban areas of Antakya, 24% of Iskenderun, and 8% of Adana were affected by the earthquake calculated by log ratio between an average pre-event coherence image and post-event coherence image which indicates intensity of coherence changes.

In the city of Mariupol, there was decreasing of coherence in different parts of the city and different periods of time in our study. At the beginning of invasion in late February 2022, there was almost no change appeared in the results. Then, changes appeared to be more intense from middle March. The media reported that on the first few days, the fighting was limited to the outskirts of the city. The city was well defended from the east, where the Ukrainians expected the Russians to launch an attack. But there was no preparation for an invasion from the west. Russian troops poured across the narrow isthmus from Crimea towards Mariupol, and within a few days, the city was encircled (Walker et al., 2023). On 3 March, the mayor of Mariupol

said Russian forces had blockaded the city, cut off water, power and food (Bisset, 2022).

The result of 4 and 16 March showed damage mostly in the western part of the city, some on the eastern edge of the area of interest, and nearby the area of Azovstal industrial site. The media reported that after the blockade of the city, the city had been shelled. There was the hospital strike on 9 March, followed by taking over the largest hospital in Mariupol on 15 March and the theatre bombing on 16 March (The Straits Times, 2022).

The result of 16 and 28 March showed the damage clustered in the city centre while the media reported that on 18 March, the Russian forces entered the city centre with heavy fighting followed by a school bombing on 20 March. Then, on 28 March, the mayor's office of Mariupol estimates that around 90 per cent of the buildings have been damaged and 40 per cent destroyed (Al Jazeera, 2022; The Straits Times, 2022).

The results showed the most significant change of coherence in the city centre and the area of Azovstal industrial site which located in the middle part of the city on the coast of the sea from early April to middle May 2022. The media reported that in the middle of April, the army leadership orders all remaining units of Ukrainian troops defending the city to regroup at Azovstal while Russia said it had controlled the urban parts of the city (The Straits Times, 2022; Walker et al., 2023). Then the heavy fighting focused on the Azovstal industrial site as thousands of Ukrainian fighters uses the plant and its sprawling network of underground tunnels as the final shelter and stronghold as illustrated in Figure 42.

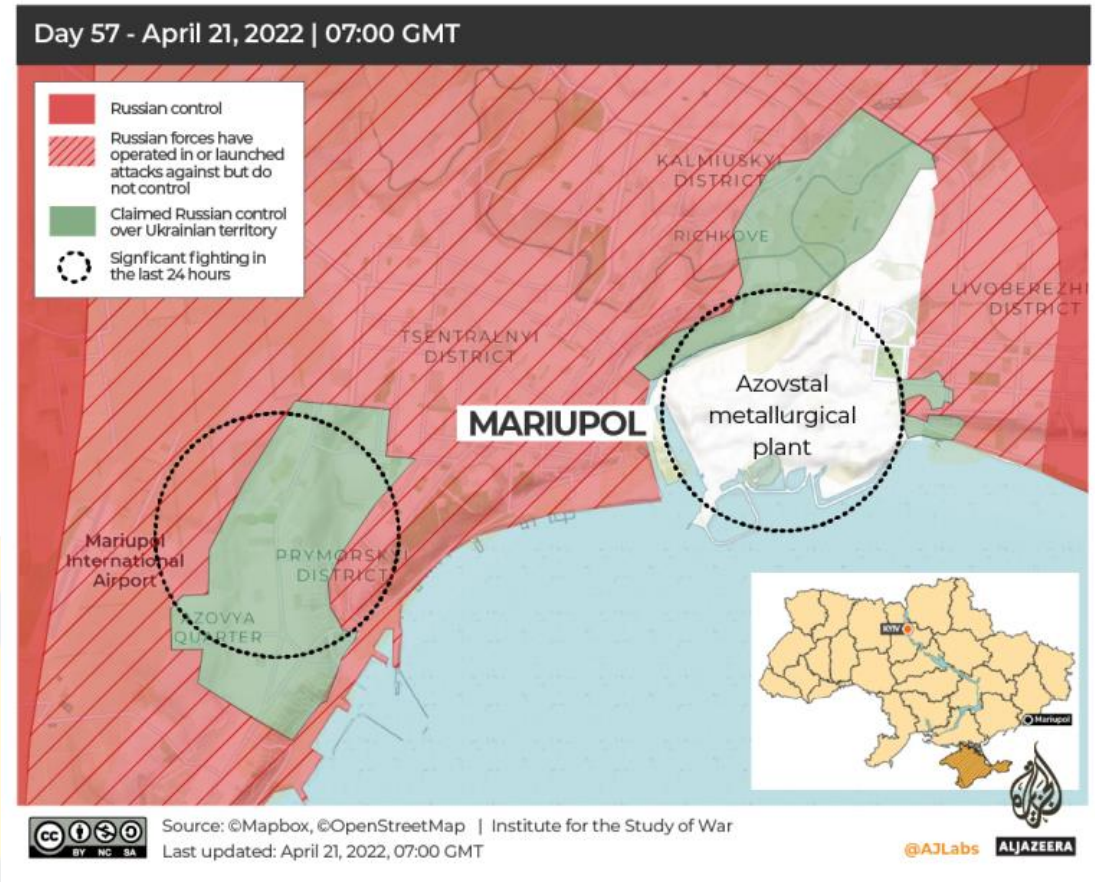

Figure 42 The territory map of Mariupol produced by Al Jazeera (2022).

The fighting continued until the Ukrainian fighters surrendered and Russia claimed to take full control of the Azovstal steel plant on 20 May (Al Jazeera, 2022; Bisset, 2022). From late May, there was no large cluster of change in the city and the area of Azovstal industrial site appeared high coherence value more than other parts of the city. The calculation from the results showed that 34.01% of the urban areas were affected from the beginning of the invasion until June 2022.

However, the percentage of damage calculated from log ratio images seems to be lower than the reports from media since we calculated all pixels in each area of interest. These areas of interest include not only buildings but also parks, gardens, vegetation, water bodies, and bare lands. There were studies that integrated the coherence images to street blocks and land use classification which can be used to analyse affected coherence in the different land use. In this way, it is more appropriate

in an urban set-up as street blocks are relate to objects in the real world (Washaya et al., 2018).

As seen from the results, there are damages detected by the CCD technique in some areas that could not be seen by looking at Google Earth images. Those could be small changes since the CCD technique is able to detect even small changes. On the other hand, those changes could be affected by a variety of factors which caused coherence loss. Moreover, coherence is also suffering from speckling, which requires the combination of several pixels to get reliable results (Balz et al., 2018). It is essential to find methods to improve detection and assessment of the intensity of damage.

Urban areas naturally have high coherence over a long period, instant changes of coherence can indicate changes on that area. On the other hand, coherence is uncertain in non-urban areas which often show rapid coherence dropping in a short period as shown in the results that in the coherence image, vegetation appeared to be poor coherence while buildings have very high coherence. Many researchers used changes in SAR backscattering intensity and coherence for building damage assessment. The CCD technique makes use of the similarity or difference of the phase properties of SAR images in order to detect changes after a disaster (Washaya et al., 2018). It is suitable to identify changes in urban areas. The coherence information is also more sensitive to minor ground changes than intensity information, so the CCD technique is useful to identify even small changes (Ge et al., 2020). However, it is generally acknowledged that speckle effects, and single-pixel damage classification from the medium resolution SAR image can lead to ineffective results while the damage assessment at a block level can achieve effective results (Aimaiti et al., 2022; Dell'Acqua & Gamba, 2012). Moreover, using high-resolution SAR images such as TerraSAR-X and COSMO-SkyMed accurate single-building scale damage mapping can achieve detailed single-building scale damage mapping while medium resolution SAR images like Sentinel-1 can detect damage of large buildings.

Conclusion

In this study, we introduced the concept of using the coherence change detection technique (CCD) with Sentinel-1 images and we focused on urban areas which damaged from the earthquake in three cities of Turkey including Antakya and Iskenderun in Hatay province, and Adana in Adana province. We also focused on damage of urban areas occurred by war in Mariupol of Ukraine. For each study area, we used SAR images of three months before an event to generate an average pre-event coherence image as a master image to compare with one image after the event. In case of Mariupol, we used several post event images to compare with an average pre-event coherence image. Since the event lasted for three months, we used 10 post event coherence images to find changes of coherence in the period of each post coherence image. We applied a log ratio to find the intensity of coherence changes after an event occurred in each study area.

The study showed that the pre-event coherence value of urban areas was high then turned to low after the earthquake, especially in the city of Antakya, which is one of the most affected cities as the post event coherence image showed reduction of coherence in all over the city, while the post event coherence of Iskenderun showed loss of coherence mostly in the north-western part of the city as this city was less affected than Antakya. The coherence of Adana slightly decreased after the earthquake as this city was least affected by the earthquake compared to other cities of our study. In the city of Mariupol, the study showed loss of coherence in areas that were affected by war in each period. There were gradually changes in the beginning of the invasion, then a lot of changes occurred in middle March to middle May 2022 and the most intense changes happened in the city centre and the Azovstal industrial site. However, there also were widespread changes all over the urban areas.

The CCD technique is a useful method in applying to measure changes in urban areas affected by disasters like earthquakes and wars. However, the CCD technique is not suitable to apply in areas that covered with vegetation. Moreover, the global accessibility of Sentinel-1 data is useful to monitor any kind of disasters.

REFERENCES

Aimaiti, Y., Sanon, C., Koch, M., Baise, L. G., & Moaveni, B. (2022). War Related Building Damage Assessment in Kyiv, Ukraine, Using Sentinel-1 Radar and Sentinel-2 Optical Images. *Remote Sensing*, *14*(24), 6239.

Al Jazeera. (2022). *Timeline: Russia's siege of Ukraine's Mariupol*. Al Jazeera. Retrieved from https://www.aljazeera.com/news/2022/3/31/timeline-russias-siege-of-ukraines-port-city-of-mariupol

Balz, T., Washaya, P., & Jendryke, M. (2018). Urban change monitoring using globally available SENTINEL-1 imagery. In *2018 International Workshop on Big Geospatial Data and Data Science (BGDDS)* (pp. 1-4) IEEE.

Bisset, V. (2022). *In pictures: How the Mariupol siege unfolded*. The Washington Post. Retrieved from https://www.washingtonpost.com/world/2022/05/21/ukraine-mariupol-azovstal-siege-timeline/

Boloorani, A. D., Darvishi, M., Weng, Q., & Liu, X. (2021). Post-War Urban Damage Mapping Using InSAR: The Case of Mosul City in Iraq. *ISPRS International Journal of Geo-Information*, *10*(3), 140.

Bouaraba, A., Acheroy, M., & Closson, D. (2013). Coherent change detection performance using high-resolution SAR images. *International Journal of Engineering Research & Technology (IJERT)*, *2*(11), 3160-3166.

Britannica. (2022). *Mariupol*. Encyclopaedia Britannica. Retrieved from https://www.britannica.com/place/Mariupol

Britannica. (2023a). *Antioch*. Encyclopaedia Britannica. Retrieved from https://www.britannica.com/place/Antioch-modern-and-ancient-city-south-central-Turkey

Britannica. (2023b). *İskenderun*. Encyclopaedia Britannica. Retrieved from https://www.britannica.com/place/Iskenderun-Turkey

Cappucci, M. (2023). *What triggered the Turkey quakes? Why was the second so big? Key questions, answered.* Retrieved from https://www.washingtonpost.com/weather/2023/02/07/earthquake-turkey-syria-causes-damage/

Closson, D., & Milisavljevic, N. (2017). InSAR coherence and intensity changes

detection. *Mine Action-The Research Experience of the Royal Military Academy of Belgium*.

Damini, A., Mantle, V., & Davidson, G. (2013). A new approach to coherent change detection in VideoSAR imagery using stack averaged coherence. In *2013 IEEE Radar Conference (RadarCon13)* (pp. 1-5) IEEE.

Dell'Acqua, F., & Gamba, P. (2012). Remote sensing and earthquake damage assessment: Experiences, limits, and perspectives. *Proceedings of the IEEE, 100*(10), 2876-2890.

EastFruit. (2023). *International logistics: Turkish port "Iskenderun" severely damaged due to the earthquake*. Retrieved from https://east-fruit.com/en/news/international-logistics-turkish-port-iskenderun-severely-damaged-due-to-the-earthquake/

ElGharbawi, T., & Zarzoura, F. (2021). Damage detection using SAR coherence statistical analysis, application to Beirut, Lebanon. *ISPRS Journal of Photogrammetry and Remote Sensing, 173*, 1-9.

Estrin, D., Harbage, C., Balaban, S., & Yilmazel, G. (2023). *Turkey's Antakya is in ruins after the quake, erasing cultural and religious heritage*. Retrieved from https://www.npr.org/2023/02/25/1158693549/turkey-earthquake-antakya-antioch-religions-cultural-heritage-ruins

European Space Agency. (2012). *Copernicus: Sentinel-1*. European Space Agency. Retrieved from https://www.eoportal.org/satellite-missions/copernicus-sentinel-1#copernicus-sentinel-1--the-sar-imaging-constellation-for-land-and-ocean-services

European Space Agency. (2020). *SNAP desktop*. Retrieved from https://www.esa.int/ESA_Multimedia/Images/2020/04/SNAP_desktop

European Space Agency. (n.d.-a). *Band Maths Expression Editor*. Retrieved from https://seadas.gsfc.nasa.gov/help-8.2.0/desktop/ExpressionEditor.html

European Space Agency. (n.d.-b). *Data Products*. Retrieved from https://sentinels.copernicus.eu/web/sentinel/missions/sentinel-1/data-products

European Space Agency. (n.d.-c). *InSAR processing: a mathematical approach*. Retrieved from https://www.esa.int/esapub/tm/tm19/TM-19_ptC.pdf

European Space Agency. (n.d.-d). *Interferometric Wide Swath*. Retrieved from https://sentinel.esa.int/web/sentinel/user-guides/sentinel-1-sar/acquisition-modes/interferometric-wide-swath

European Space Agency. (n.d.-e). *SNAP*. Retrieved from https://earth.esa.int/eogateway/tools/snap

Fakhri, F., & Gkanatsios, I. (2021). Integration of Sentinel-1 and Sentinel-2 data for change detection: A case study in a war conflict area of Mosul city. *Remote Sensing Applications: Society and Environment*, *22*, 100505.

Ge, P., Gokon, H., & Meguro, K. (2020). A review on synthetic aperture radar-based building damage assessment in disasters. *Remote Sensing of Environment*, *240*, 111693.

Guida, L., Boccardo, P., Donevski, I., Lo Schiavo, L., Molinari, M., Monti-Guarnieri, A., Oxoli, D., & Brovelli, M. (2018). Post-Disaster Damage Assessment Through Coherent Change Detection on SAR Imagery. *International Archives of the Photogrammetry, Remote Sensing & Spatial Information Sciences*, *42*(3).

Gunasekera, R., Ishizawa Escudero, O. A., Daniell, J. E., Pomonis, A., Macabuag, J. L. D. C., Brand, J., Schaefer, A., Romero, R., Esper, S., Otálora, S. G., Khazai, B., & Cox, K. D. (2023). *Global Rapid Post-Disaster Damage Estimation (GRADE) Report : February 6, 2023 Kahramanmaraş Earthquakes - Türkiye Report (English)*. World Bank Group. Retrieved from http://documents.worldbank.org/curated/en/099022723021250141/P1788430aeb62f08009b2302bd4074030fb

Jendryke, M., Balz, T., & Liao, M. (2016). Observing urban built-up change in shanghai with SAR imagery. In *2016 IEEE International Geoscience and Remote Sensing Symposium (IGARSS)* (pp. 1788-1791) IEEE.

Kirac, N. (2023). *After Earthquake, a Turkish Journalist Debates Leaving Home*. The New York Times. Retrieved from https://www.nytimes.com/2023/03/29/insider/after-earthquake-a-turkish-journalist-debates-leaving-home.html

Mastro, P., Masiello, G., Serio, C., & Pepe, A. (2022). Change Detection Techniques with Synthetic Aperture Radar Images: Experiments with Random Forests and

Sentinel-1 Observations. *Remote Sensing*, *14*(14), 3323.

NASA. (2023). *What Part of the Earth was Mapped?* NASA. Retrieved from https://www2.jpl.nasa.gov/srtm/coverage.html

Office of the High Commissioner United Nations Human Rights. (2022a). *High Commissioner updates the Human Rights Council on Mariupol, Ukraine*. Office of the High Commissioner United Nations Human Rights. Retrieved from https://www.ohchr.org/en/statements/2022/06/high-commissioner-updates-human-rights-council-mariupol-ukraine

Office of the High Commissioner United Nations Human Rights. (2022b). *UN experts call for international investigation into 2020 Beirut explosion*. Office of the High Commissioner United Nations Human Rights. Retrieved from https://www.ohchr.org/en/press-releases/2022/08/un-experts-call-international-investigation-2020-beirut-explosion

Plank, S. (2014). Rapid damage assessment by means of multi-temporal SAR—A comprehensive review and outlook to Sentinel-1. *Remote Sensing*, *6*(6), 4870-4906.

Psaropoulos, J. (2022). *Timeline: Six months of Russia's war in Ukraine*. Aljazeera. Retrieved from https://www.aljazeera.com/news/2022/8/24/timeline-six-months-of-russias-war-in-ukraine

Putri, A. F. S., Widyatmanti, W., & Umarhadi, D. A. (2022). Sentinel-1 and Sentinel-2 data fusion to distinguish building damage level of the 2018 Lombok Earthquake. *Remote Sensing Applications: Society and Environment*, *26*, 100724.

Şeşetyan, K., Stucchi, M., Castelli, V., & Gómez Capera, A. A. (2023). Kahramanmaraş-Gaziantep Türkiye M7. 7 Earthquake, 6 February 2023 (04: 17 GMT+ 03: 00) Large historical earthquakes of the earthquake-affected region: a preliminary report.

Swamy, K. (2015). *Re: Why do we take the natural log of book-to-market ratios, as used in FAMA & French (1992) and Sloan (1996) papers?* Retrieved from https://www.researchgate.net/post/Why-do-we-take-the-natural-log-of-book-to-market-ratios-as-used-in-FAMA-French-1992-and-Sloan-1996-

papers/55204833d3df3e6c648b4665/citation/download

The Straits Times. (2022). *Timeline: Russia's siege of the Ukrainian city of Mariupol*. Retrieved from https://www.straitstimes.com/world/europe/timeline-russias-siege-of-the-ukrainian-city-of-mariupol

The World Bank. (2022). *Ukraine Recovery and Reconstruction Needs Estimated $349 Billion*. The World Bank. Retrieved from https://www.worldbank.org/en/news/press-release/2022/09/09/ukraine-recovery-and-reconstruction-needs-estimated-349-billion

United Nations. (2010). *Earthquakes the deadliest of all disasters during past decade – UN official*. United Nations. Retrieved from https://news.un.org/en/story/2010/01/327892-earthquakes-deadliest-all-disasters-during-past-decade-un-official

United Nations. (2022). *The UN and the war in Ukraine: key information*. United Nation. Retrieved from https://unric.org/en/the-un-and-the-war-in-ukraine-key-information/

United Nations Office for the Coordination of Humanitarian Affairs. (2023). *Turkey-Earthquake: Emergency Situation Report (12.04.2023)*. United Nations Office for the Coordination of Humanitarian Affairs Retrieved from https://reliefweb.int/report/turkiye/turkey-earthquake-emergency-situation-report-12042023

United Office for Disaster Risk Reduction. (2020). *The human cost of disasters: an overview of the last 20 years (2000-2019)*. United Office for Disaster Risk Reduction. Retrieved from https://www.undrr.org/publication/human-cost-disasters-overview-last-20-years-2000-2019

Walker, S., Koshiw, I., Sauer, P., Risberg, M., Cookman, L., & Harding, L. (2023). *Mariupol The ruin of a city*. Retrieved from https://www.theguardian.com/world/ng-interactive/2023/feb/23/mariupol-the-ruin-of-a-city

Washaya, P., & Balz, T. (2018). SAR coherence change detection of urban areas affected by disasters using sentinel-1 imagery. *The International Archives of the Photogrammetry, Remote Sensing and Spatial Information Sciences, 42*, 1857-

1861.

Washaya, P., Balz, T., & Mohamadi, B. (2018). Coherence change-detection with sentinel-1 for natural and anthropogenic disaster monitoring in urban areas. *Remote Sensing*, *10*(7), 1026.

White, J., Gates, G., Leatherby, L., Reinhard, S., & Abraham, L. (2023). *Thousands of buildings collapsed in one Turkish city. Thousands more may have to come down*. The Seattle Times. Retrieved from https://www.seattletimes.com/nation-world/thousands-of-buildings-collapsed-in-one-turkish-city-thousands-more-may-have-to-come-down/

Yamazaki, F., & Matsuoka, M. (2007). Remote sensing technologies in post-disaster damage assessment. *Journal of Earthquake and Tsunami*, *1*(03), 193-210.

มหาวิทยาลัยบูรพา
BURAPHA UNIVERSITY

BIOGRAPHY

NAME	Methichai Obom
DATE OF BIRTH	4 May 1990
PLACE OF BIRTH	Nakhon Sawan, Thailand
PRESENT ADDRESS	127/1507 Moo 3, Sir Samman Road, Ban Mai, Pak Kret, Nonthaburi, Thailand
POSITION HELD	Technical Officer, Space Affairs Center, Defence Information and Space Technology Department, Thailand
EDUCATION	Bachelor of Engineering (Computer Engineering), Chiang Mai University, Thailand